nature metabolism

LETTERS

https://doi.org/10.1038/s42255-020-00315-1

Check for updates

KRAS-regulated glutamine metabolism requires UCP2-mediated aspartate transport to support pancreatic cancer growth

Susanna Raho[1,11], Loredana Capobianco[2,11], Rocco Malivindi[3,11], Angelo Vozza[1,11], Carmela Piazzolla[1], Francesco De Leonardis[1], Ruggiero Gorgoglione[1], Pasquale Scarcia[1], Francesca Pezzuto[2], Gennaro Agrimi[1], Simona N. Barile[1], Isabella Pisano[1], Stephan J. Reshkin[1], Maria R. Greco[1], Rosa A. Cardone[1], Vittoria Rago[3], Yuan Li[1,4], Carlo M. T. Marobbio[1], Wolfgang Sommergruber[5], Christopher L. Riley[6], Francesco M. Lasorsa[1,7], Edward Mills[8], Maria C. Vegliante[9], Giuseppe E. De Benedetto[10], Deborah Fratantonio[1], Luigi Palmieri[1,7], Vincenza Dolce[3] ✉ and Giuseppe Fiermonte[1,7] ✉

The oncogenic *KRAS* mutation has a critical role in the initiation of human pancreatic ductal adenocarcinoma (PDAC) since it rewires glutamine metabolism to increase reduced nicotinamide adenine dinucleotide phosphate (NADPH) production, balancing cellular redox homeostasis with macromolecular synthesis[1,2]. Mitochondrial glutamine-derived aspartate must be transported into the cytosol to generate metabolic precursors for NADPH production[2]. The mitochondrial transporter responsible for this aspartate efflux has remained elusive. Here, we show that mitochondrial uncoupling protein 2 (UCP2) catalyses this transport and promotes tumour growth. UCP2-silenced *KRAS*^{mut} cell lines display decreased glutaminolysis, lower NADPH/NADP$^+$ and glutathione/glutathione disulfide ratios and higher reactive oxygen species levels compared to wild-type counterparts. UCP2 silencing reduces glutaminolysis also in *KRAS*^{WT} PDAC cells but does not affect their redox homeostasis or proliferation rates. In vitro and in vivo, UCP2 silencing strongly suppresses *KRAS*^{mut} PDAC cell growth. Collectively, these results demonstrate that UCP2 plays a vital role in PDAC, since its aspartate transport activity connects the mitochondrial and cytosolic reactions necessary for *KRAS*^{mut} rewired glutamine metabolism[2], and thus it should be considered a key metabolic target for the treatment of this refractory tumour.

Energy production, redox homeostasis and macromolecular synthesis in most cancer cells rely on glutamine (Gln) consumption[3,4]. The main metabolites derived from mitochondrial Gln oxidation are aspartate (Asp) and malate (Mal)[4,5], which are transported to the cytosol, where Asp is used for nucleotide and protein synthesis, and Mal is used to generate NADPH for reductive biosynthesis and cellular redox homeostasis[4]. In PDAC, oncogenic *KRAS* induces metabolic rewiring of the pentose phosphate pathway such that ribose 5-phosphate biogenesis is decoupled from NADPH production[1]. This metabolic alteration encourages a Gln addiction[2,6]. To fulfil the NADPH needs, *KRAS* triggers rewired Gln metabolism, wherein mitochondrial Gln-derived Asp, once transported to the cytosol, is converted to oxaloacetate (OA), Mal and finally to pyruvate (Pyr) to produce NADPH[2] (Fig. 1a). Although this pathway has been known[2,7,8], the mitochondrial carrier responsible for Asp efflux from mitochondria is missing. One possible candidate is UCP2 (Fig. 1a).

We recently showed that bacterially expressed and refolded UCP2 in artificial lipid vesicles can catalyse the transport of Asp against phosphate plus a proton[9]. Furthermore, UCP2 is upregulated at the translational level by Gln[10,11], required for macrophage and HepG2 Gln oxidation[9,12] and overexpressed in PDAC compared with healthy tissue (Extended Data Fig. 1a). To assess the role of UCP2 in PDAC-rewired Gln metabolism, we silenced *UCP2* using RNA interference. Four PDAC cell lines, two *KRAS*^{mut}, Patu8988T and Panc1, and two *KRAS*^{WT}, BxPC3 and KP2, were used. The efficiency of silencing was verified at both the transcript and protein levels (Extended Data Fig. 1b,c). Although all four cell lines showed significant differences in *UCP2* transcript abundance, we did not find a proportional correspondence at the protein level (Extended Data Fig. 1c,d). This confirmed that *UCP2* is regulated at both the transcriptional and translational levels[13]. UCP2 silencing did not alter the expression of other members of the mitochondrial UCP subfamily (UCP3–5)[14], which are expressed at levels much lower than those of UCP2 (Extended Data Fig. 1e,f) and UCP1 was absent in all cell lines. Detergent-solubilized mitochondrial extracts from *UCP2*-silenced cells reconstituted into artificial lipid vesicles[9] did not catalyse any significant Asp/phosphate (Pi) transport activity (Extended Data Fig. 1g). We then assayed the effect of UCP2 silencing

[1]Department of Bioscience, Biotechnology and Biopharmaceutics, University of Bari, Bari, Italy. [2]Department of Biological and Environmental Sciences and Technologies, University of Salento, Lecce, Italy. [3]Department of Pharmacy, Health and Nutritional Sciences, University of Calabria, Rende, Italy. [4]Faculty of Biological Engineering, Sichuan University of Science and Engineering, Yibin, China. [5]Boehringer Ingelheim RCV GmbH & Co KG, Vienna, Austria. [6]Department of Cancer Biology, Dana-Farber Cancer Institute, Boston, MA, USA. [7]Institute of Biomembranes and Bioenergetics, Consiglio Nazionale delle Ricerche, Bari, Italy. [8]Division of Pharmacy and Toxicology, College of Pharmacy, The University of Texas at Austin, Austin, TX, USA. [9]Hematology and Cell Therapy Unit, Istituto di Ricovero e Cura a Carattere scientifico-Istituto Tumori 'Giovanni Paolo II', Bari, Italy. [10]Dipartimento Beni Culturali, University of Salento, Lecce, Italy. [11]These authors contributed equally: Susanna Raho, Loredana Capobianco, Rocco Malivindi, Angelo Vozza. ✉e-mail: vincenza.dolce@unical.it; giuseppe.fiermonte@uniba.it

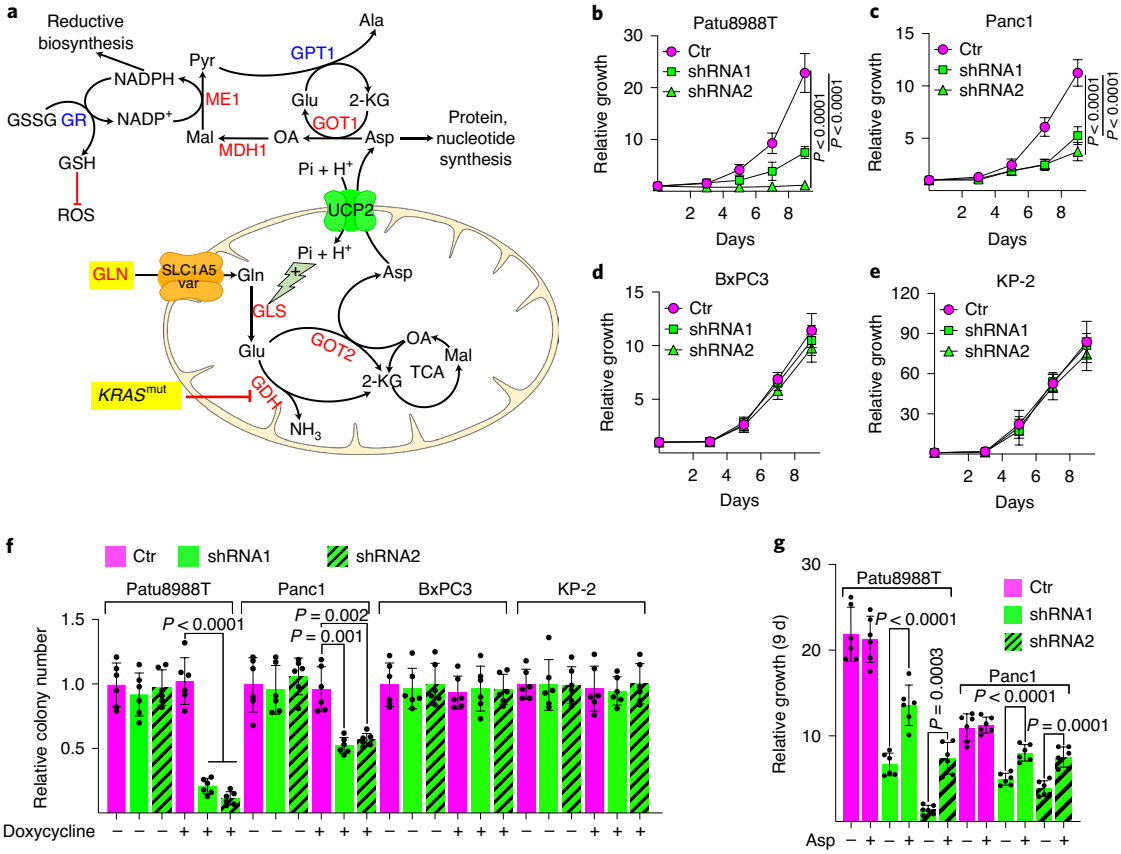

Fig. 1 | UCP2 silencing reduces the availability of cytosolic Asp in PDAC cell lines. a, The rewired Gln metabolism induced by *KRAS*^{mut} in PDAC[2]. The enzymes involved in *KRAS*-dependent Gln metabolism are shown in red[2]. **b**–**f**, UCP2 silencing reduces the proliferation rate and the clonogenic capacity of *KRAS*^{mut} PDAC cells. An appropriate number of cells was plated in specific growth media supplemented with 10 mM glucose, 2 mM glutamine and 10% FCS. The next day, the media were exchanged for D5030 medium supplemented with 10 mM glucose, 2 mM glutamine, 10% dFCS and doxycycline. At the indicated time points, cells were counted with an automated Scepter cell counter (**b**–**e**). The histogram data refer to Ctr shRNA transfected cells with or without doxycycline (**f**). **g**, Asp in the medium partially rescues the proliferation growth defect of UCP2-silenced Patu8988T and Panc1 cells. Doxycycline was always present in **b**–**e** and **g**. GR, glutathione reductase; ME1, NADP-dependent malic enzyme; GPT1, glutamate pyruvate transaminase 1; GOT1/GOT2, glutamate oxaloacetate transaminase 1/2; GDH, glutamate dehydrogenase; MDH1, malate dehydrogenase, cytoplasmic. Values represent the means ± s.d. of two biologically independent triplicates. Statistical significance was calculated by unpaired two-tailed Student's *t*-test. Welch correction was applied to **b**,**f** and shRNA2 (−Asp) versus shRNA2 (+Asp) (**g**).

on cell proliferation and colony-forming capacity. All experiments were done in the presence of Gln since *UCP2* expression is Gln dependent[10,11] (Extended Data Fig. 1i). To identify the defect induced by the loss of mitochondrial efflux of Asp by UCP2 silencing, all experiments were carried out in the presence of dialysed FCS similar to that previously used to map the *KRAS*-rewired Gln metabolism[2]. UCP2 silencing significantly decreased the proliferation rate and colony-forming capacity of *KRAS*^{mut} cells, Patu8988T and Panc1, but not *KRAS*^{WT} cells, BxPC3 and KP2 (Fig. 1b–f and Extended Data Fig. 2a–d). The addition of Asp to medium partially but significantly rescued the previously observed defects (Fig. 1g and Extended Data Fig. 2a,b,e,f), confirming that UCP2 silencing depleted cytosolic Asp.

Interestingly, the proliferation defect induced by UCP2 silencing was also partially rescued by the addition of glutamate (Glu) to medium (Extended Data Fig. 2g). Since Glu cannot produce NADPH in the cytosol (Fig. 1a), we hypothesized that Glu enters mitochondria through the mitochondrial Asp/Glu carrier (AGC1) where it produces Asp by following the same reaction pathways as mitochondrial Glu derived from Gln. Importantly, AGC is expressed in the four PDAC cell lines and UCP2 silencing does not alter its expression (Extended Data Fig. 2h). Since AGC is a strict counter-exchanger, the entry of Glu occurs only if Asp exits[15]. The export of Asp by AGC requires the entry of Glu (Extended Data Fig. 2i) but this would result in the accumulation of four-carbon Gln-derived metabolites in the matrix, inhibiting glutaminolysis[16]. As such, we hypothesized this pathway is only used when there are high concentrations of cytosolic Glu. Furthermore, AGC transport activity is crucial for cell proliferation during Gln starvation and its loss sensitizes tumours to CB-389, a glutaminase (GLS) inhibitor[17]. Under Gln-replete conditions in PDAC cells, Gln is transported into the matrix through the mitochondrial Gln transporter, SLC1A5_var, producing Asp in the matrix[18]; this requires a mitochondrial carrier able to catalyse a net efflux of Asp. UCP2 is the only known mitochondrial carrier able to catalyse the exchange of aspartate against P_i plus a proton[9]. Interestingly, silencing of SLC1A5_var and *UCP2* reduce gemcitabine resistance of PDAC cells[18,19].

The addition of reduced glutathione (GSH) or *N*-acetylcysteine (NAC) completely restored the growth defects seen in the absence of UCP2 (Fig. 2a and Extended Data Fig. 3a). This confirmed that the cytosolic depletion of Asp in the *KRAS*^{mut} PDAC cells, induced by UCP2 silencing, decreased GSH availability[2] and altered cellular redox homeostasis. To dissect this point, we explored the effect of UCP2 silencing on the glutathione/glutathione disulfide (GSH/

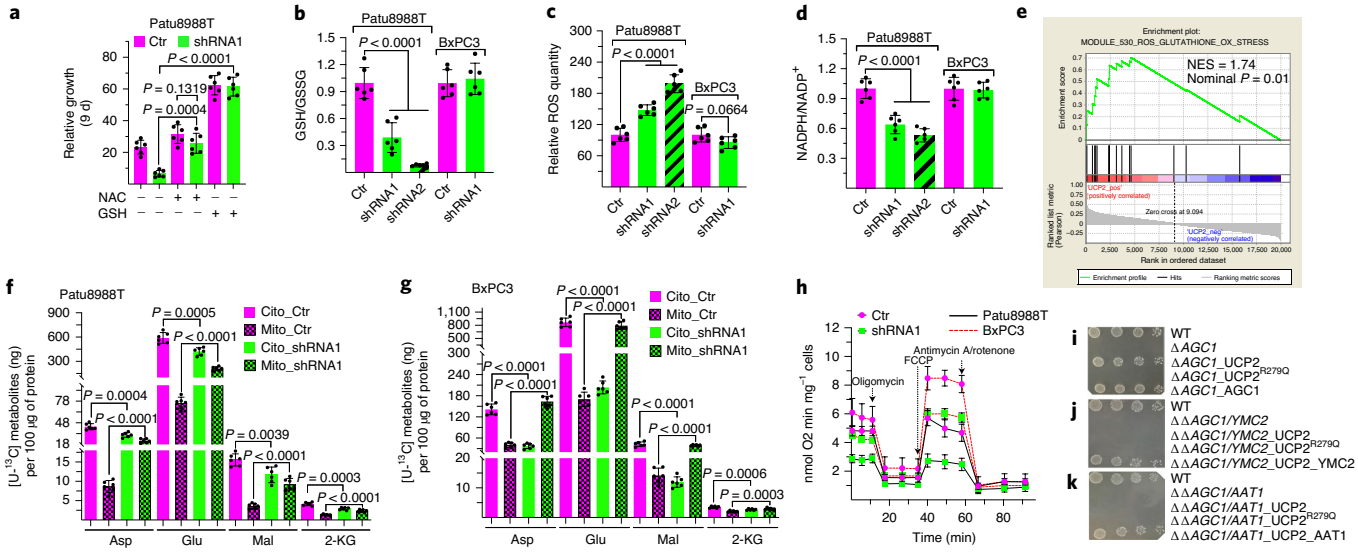

Fig. 2 | The UCP2 Asp/P_i activity connects the mitochondrial and cytosolic reactions necessary for rewired Gln metabolism and regulates the redox homeostasis of PDAC cells. a, GSH or NAC in the medium fully rescues the growth defect of *UCP2*-silenced Patu8988T cells. **b**, UCP2 silencing reduces the GSH/GSSG ratio only in $KRAS^{mut}$ cells. **c**, UCP2 silencing increases ROS levels only in $KRAS^{mut}$ cells. **d**, UCP2 silencing reduces the NADPH/$NADP^+$ ratio only in $KRAS^{mut}$ cells. The histogram data refer to Ctr^{shRNA}-transfected cells (**b**–**d**). **e**, In PDAC, *UCP2* expression levels are associated with those of genes involved in redox homeostasis. The GSEA panel shows the enrichment of gene sets related to *UCP2* expression in roughly 300 PDAC primary tumour samples from the E-MTAB-6134 dataset. NES, normalized enrichment score. **f**,**g**, UCP2 silencing alters the cytosol/matrix distribution of the Gln-derived metabolites in Patu8988T (**f**) and BxPC3 (**g**) PDAC cells. **h**, *UCP2*-silenced PDAC cells show a reduced OCR in the presence of Gln; the values represent the means ± s.d. of three biologically independent experiments. **i**–**k**, UCP2 functions as an Asp/P_i exchanger in yeast cells. The culture concentration of various transformed yeast strains was normalized in water to an optical density at 600 nm of 0.4. Four serial diluitions of the different cell models expressing UCP2 or $UCP2^{R279Q}$ were spotted onto YP plates in the presence of 0.5 mM oleate. Plates were placed at 30 °C, and pictures were taken after 3 days to show yeast growth performance. **a**–**d**,**f**,**g**, The values represent the means ± s.d. of two biologically independent triplicates. Statistical significance was calculated by unpaired two-tailed Student's *t*-test. Welch correction was applied to sh. 1 (−NAC) versus shRNA1 (+NAC), shRNA1 (−GSH) versus shRNA1 (+GSH) (**a**), control versus shRNA2 (**b**), $Mito\_Ctr^{NI}$ versus $Mito\_shRNA1^{NI}$ (Glu) (**f**), $Cito\_Ctr^{NI}$ versus $Cito\_shRNA1^{NI}$, $Mito\_Ctr^{NI}$ versus $Mito\_shRNA1^{NI}$ (Glu), $Cito\_Ctr^{NI}$ versus $Cito\_shRNA1^{NI}$ (Mal) (**g**).

GSSG) ratio. As expected, UCP2 silencing decreased the GSH/GSSG ratios in the Patu8988T and Panc1 but not in $KRAS^{WT}$ cells (Fig. 2b and Extended Data Fig. 3b). These results were confirmed by the increase in reactive oxygen species (ROS) found in *UCP2*-silenced $KRAS^{mut}$ cells (Fig. 2c and Extended Data Fig. 3c–i). Remarkably, UCP2 silencing slightly decreased ROS in the two $KRAS^{WT}$ cells. Because *KRAS*-dependent Gln metabolism requires cytosolic Asp derived from mitochondrial Gln oxidation to reduce glutathione using cytosolic NADPH[2], we tested if the NADPH/$NADP^+$ ratio was decreased by UCP2 silencing. The results reported in Fig. 2d and Extended Data Fig. 3j confirmed that the lower GSH/GSSG ratio found in the Patu8988T and Panc1 cells correlated with a lower NADPH/$NADP^+$ ratio, whereas the NADPH/$NADP^+$ ratio in $KRAS^{WT}$ cells was unaffected by UCP2 silencing. In support of these results, gene set enrichment analysis (GSEA) carried out on the gene expression profile (GEP) of roughly 300 PDAC primary tumour samples and 43 PDAC cell lines showed a significant association of *UCP2* expression with genes involved in GSH metabolism, oxidoreductase activity acting on NADH or NADPH, cellular response to oxidative stress and ROS metabolism (Fig. 2e, Extended Data Fig. 3k,l and Supplementary Table 1). To gain more insight into the metabolic changes observed in PDAC cells on UCP2 silencing, we carried out a targeted metabolomic analysis using uniformly ^{13}C-labelled Gln ([U-^{13}C]Gln) as a tracer.

UCP2 silencing did not produce a significant difference in the labelling of metabolites derived from Gln utilization, that is, Glu, Asp, Mal and 2-ketoglutarate (2-KG). One explanation could be that the absence of UCP2 promotes a mitochondrial accumulation of labelled intermediates that would otherwise accumulate in the cytosol. To test this hypothesis, we fractionated cytosolic and organelle-enriched metabolite pools[20] (Extended Data Methods). In both $KRAS^{WT}$ and $KRAS^{mut}$ cells, UCP2 silencing led to an accumulation of Gln-derived metabolites in the organelle fraction and a decrease in the cytosolic fractions (Fig. 2f,g). Metabolomics data suggested that the loss of UCP2-dependent cataplerotic activity inhibited glutaminolysis in both $KRAS^{WT}$ and $KRAS^{mut}$ cells. This was confirmed by the lower oxygen consumption rate (OCR) of *UCP2*-silenced PDAC cells respiring on Gln (Fig. 2h). These results establish the crucial role of UCP2 in Gln metabolism[9,12] and the central nature of Gln in redox homeostasis in $KRAS^{mut}$ cells but not $KRAS^{WT}$ cells. These initial results demonstrate the vital role played by UCP2 in $KRAS^{mut}$ cells where rewired Gln metabolism occurs[2]. They also show that the higher levels of ROS found in *UCP2*-silenced Patu8988T and Panc1 cells are due to impaired Gln oxidation and not UCP2-mediated uncoupling activity since no difference was found in the two $KRAS^{WT}$ cell lines.

Since mammalian cell lines present a very complex metabolic system, we confirmed the role of UCP2 as a mitochondrial Asp exporter in yeast. Yeast cells require the Mal–Asp shuttle (MAS) for reduction of the cytosolic NADH derived from peroxisomal oleate oxidation[21] (Extended Data Fig. 4a). Deletion of AGC1, a mitochondrial transporter essential for the function of MAS in yeast, renders yeast cells unable to grow on oleate[21]. We hypothesized that if UCP2 catalysed the export of Asp from mitochondria in exchange for inorganic phosphate plus a proton and operated together with the yeast mitochondrial Glu/H^+ symporter (YMC2)[22], then Asp/Glu exchange activity would be restored (Extended Data Fig. 4b) along with the growth defect on

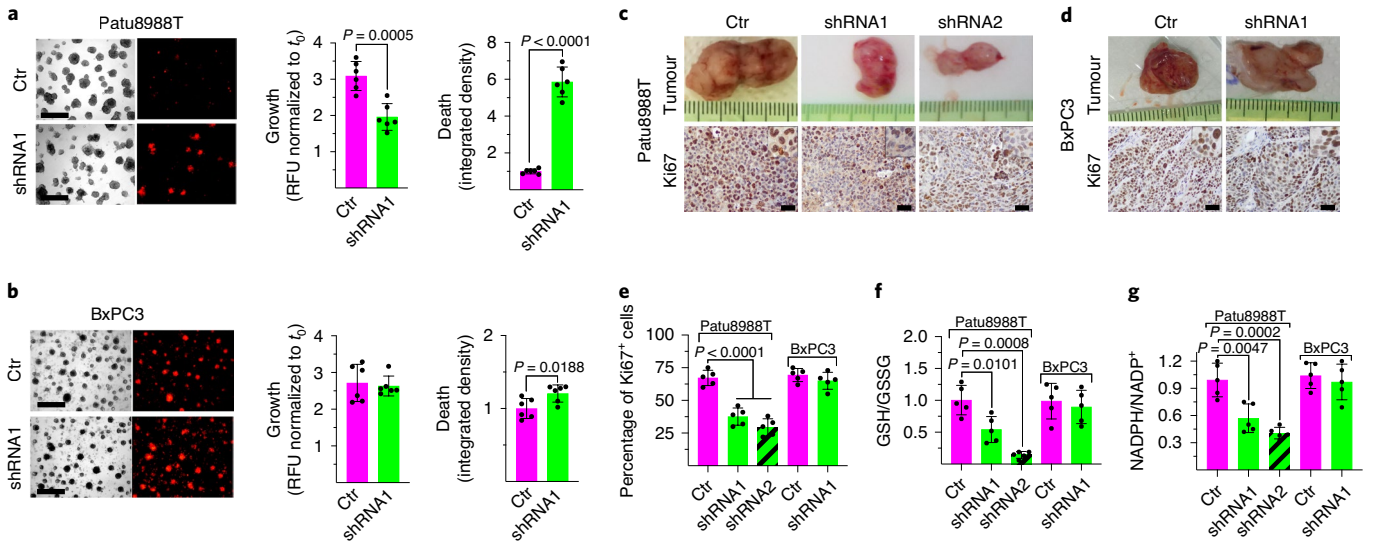

Fig. 3 | UCP2 silencing inhibits *KRAS*^{mut} PDAC cell growth in organotypic 3D and xenograft models. a,**b**, UCP2 silencing reduces growth of organotypic cultures of *KRAS*^{mut} PDAC cells. Representative microscopic images of growth and death (red signal) of Patu8988T (**a**) and BxPC3 (**b**) PDAC cells grown on 100% Matrigel extracellular matrix in the presence of doxycycline. Scale bar, 500 µm. The histograms show the growth and death of cells cultured for 7 d. The growth data were normalized to those measured at the beginning of the experiment (t_0), whereas the death data refer to the Ctr^{shRNA}-transfected cells. RFU, relative fluorescence units. **c**,**d**, UCP2 silencing inhibits the proliferation of *KRAS*^{mut} Patu8988T (**c**) and BxPC3 (**d**) PDAC cells in vivo. Representative images of tumour sizes and Ki-67 immunostaining, taken at the end point, generated by PDAC cells injected in female SCID mice ($n = 5$). The inset shows localization at higher magnification (×40). Scale bar, 25 µm. **e**, Percentage of Ki67$^+$ PDAC cells. **f**,**g**, UCP2 silencing reduces the GSH/GSSG (**f**) and NADPH/NADP$^+$ (**g**) ratios only in *KRAS*^{mut} cell xenografts; the histogram data refer to Ctr^{shRNA} xenografts. The values represent the means ± s.d. of two biologically independent triplicates (**a**,**b**) and five mice (**e**–**g**). Statistical significance was calculated by unpaired two-tailed Student's *t*-test. Welch correction was applied to death (**a**) and Ctr versus shRNA2 (**f**).

oleate of the ΔAGC1 yeast strain. To exclude possible artefacts, we constructed an inactive UCP2 mutant to use as negative control (Ctr) where arginine at position 279 was mutated to Gln. This highly conserved arginine is in the sixth transmembrane α-helix of UCP2 (refs. [23,24]) and is required for the transport activity of other mitochondrial carrier family members[25,26]. As expected, the bacterial recombinant UCP2^{R279Q} mutant did not catalyse any Asp/P_i exchange activity once reconstituted into liposomes (Extended Data Fig. 4c). Confirming our hypothesis, the ΔAGC1 yeast strain expressing UCP2 grew on oleate as the sole carbon source (Fig. 2i). Importantly, the UCP2^{R279Q} mutant, when expressed at equal levels to WT (Extended Data Fig. 4d), did not rescue the growth defect (Fig. 2i). To further demonstrate that the artificial mitochondrial Asp/Glu exchange activity was due to the synergistic functioning of UCP2 and YMC2p, we created a double mutant ΔAGC1/ΔYMC2 wherein expression of UCP2 did not restore the growth defect (Fig. 2j). Similar results were obtained when UCP2 was expressed in a yeast strain lacking the two isoforms of the oxoglutarate/Mal carrier (ODC1 and ODC2), essential components of the MAS[21,27] (Extended Data Fig. 4e). To confirm that the complementation results observed in the ΔAGC1 strain were due to the Asp transport catalysed by UCP2, we deleted Asp transaminase (AAT1), the main mitochondrial Asp-producing enzyme in the ΔAGC1 strain (Extended Data Fig. 4f). As expected, UCP2 did not rescue the growth defect of this double mutant (Fig. 2k). Together our complementation studies suggest that in vivo UCP2 cannot catalyse the Asp/Mal or Mal/oxaloacetate exchange reactions, despite our previous finding that UCP2 transports Mal, oxaloacetate, Asp and P_i[9] in vitro, since these exchange activities would have rescued the growth defect of the ΔODC1/ΔODC2 and ΔAGC1/ΔAAT1 yeast strains (Extended Data Fig. 4g,h). Taken together, our yeast complementation studies confirm that UCP2 is an Asp/P_i + H^+ transporter in vivo.

We confirmed the effects of UCP2 silencing in two relevant physiological conditions, three-dimensional (3D) organotypic cultures and xenograft models. 3D cultures were carried out on 100% Matrigel. *UCP2*-silenced *KRAS*^{mut} cells grew slower than the short hairpin RNA controls, formed smaller colonies and showed a significant increase in cell death (Fig. 3a and Extended Data Fig. 5a). The effects of UCP2 silencing in BXPC3 and KP2 (*KRAS*^{WT}) cells grown on Matrigel were similar to those previously obtained in two-dimensional cultures (Fig. 3b and Extended Data Fig. 5b) since UCP2 silencing did not alter colony size nor growth rate. It should be noted that in the two *KRAS*^{WT} cell lines, UCP2 silencing increased cell death even though the effect was less substantial than that observed in *KRAS*^{mut} cells.

To corroborate these data, we investigated the effect of UCP2 silencing in a tumour cell xenograft model. After cell implantation, the tumours were grown to a volume of 40–70 mm^3; thereafter mice were treated with doxycycline to silence *UCP2*. The loss of *UCP2* severely arrested tumour growth in mice injected with the two *KRAS*^{mut} cell lines whereas growth continued unabated in Ctr shRNA cells (Fig. 3c and Extended Data Fig. 5c,d,g,i). As expected, UCP2 silencing did not exert a significant effect on BxPC3 and KP2 xenograft growth (Fig. 3d and Extended Data Fig. 5e,f,h,i). The increased expression of Ki67 confirmed the differences in tumour size (Fig. 3c–e and Extended Data, Fig. 5g,h,j). *UCP2*-silenced *KRAS*^{mut} cell–derived tumours showed reduced GSH/GSSG and NADPH/NADP$^+$ ratios compared to those found in Ctr tumours, whereas no significant differences were found in *KRAS*^{WT} cell–derived tumours (Fig. 3f,g and Extended Data Fig. 5k,l). These results confirmed the crucial role of UCP2 in the redox homeostasis of *KRAS*^{mut} but not *KRAS*^{WT} cells in vivo.

To further verify that the growth defect observed in the *KRAS*^{mut} cells was due to UCP2 silencing, we carried out a rescue experiment by using a constitutively active shRNA (shRNA1) construct

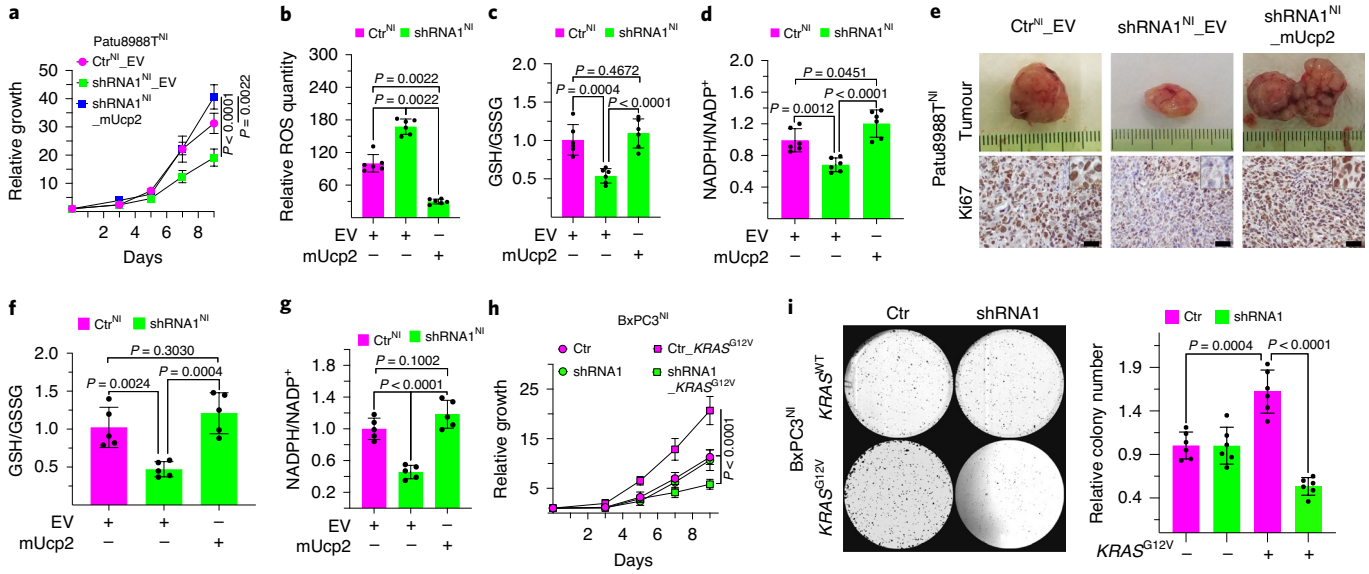

Fig. 4 | UCP2 is essential for the proliferation of PDAC cells expressing mutated *KRAS*. **a**–**d**, The expression of mUcp2 rescues the growth defect of UCP2-silenced Patu8988TNI cells (**a**) and re-establishes their redox homeostasis (**b**–**d**). The expression of mUcp2 decreases ROS levels (**b**) and increases the GSH/GSSG (**c**) and NADPH/NADP$^+$ (**d**) ratios in UCP2-silenced Patu8988T^{NI} cells. The histogram data refer to Ctr$_{shRNA}$-transfected cells carrying the empty expression vector (EV) (**b**–**d**). **e**, mUcp2 expression increases the proliferation of UCP2-silenced Patu8988T^{NI} cells in vivo. Representative images of tumour sizes and Ki-67 immunostaining, taken at the end point, generated by PDAC cells injected in female SCID mice ($n = 5$). The inset shows localization at higher magnification (×40). Scale bar, 25 µm. **f**,**g**, mUcp2 expression re-establishes redox homeostasis in xenografts. Histogram data refer to Ctr^{shRNA} xenografts carrying the EV. mUcp2 expression increases the GSH/GSSG (**f**) and NADPH/NADP$^+$ (**g**) ratios in UCP2-silenced Patu8988T^{NI}-derived xenografts. **h**,**i**, UCP2 silencing reduces the proliferation rate (**h**) and clonogenic capacity (**i**) of BxPC3 cells expressing mutated *KRAS*. The histogram data refer to Ctr^{shRNA}-transfected BxPC3 cells expressing *KRAS*^{WT} (**i**). Values represent the means ± s.d. of two biologically independent triplicates (**a**–**d**,**h**,**i**) and five mice (**f**,**g**). Statistical significance was calculated by unpaired, two-tailed Student's *t*-test (**a**,**c**,**d**,**f**–**i**) and unpaired, two-tailed Mann–Whitney *U*-test (**b**). Welch correction was applied to Ctr_*KRAS*^{G12V} versus shRNA1_*KRAS*^{G12V} (**h**). Patu8988T^{NI} and BxPC3^{NI} cells were transfected with non-inducible lentiviral plasmids.

targeting the endogenous human messenger RNA at the 5′-UTR[9] and a doxycycline-inducible lentiviral vector expressing murine Ucp2 (mUcp2). In this system, endogenous human UCP2 was silenced and the addition of doxycycline induced the expression of mUcp2. The efficiency of UCP2 silencing was slightly lower than that obtained with the inducible system (Extended Data Fig. 1c,h), whereas the addition of doxycycline greatly induced the expression of mUcp2, bringing protein expression and the Asp/P$_i$ transport activity to a level comparable to that of Patu8988T cells transfected with the Ctr$_{shRNA}$ (Extended Data Fig. 1c,h,g). mUcp2 expression restored proliferation and clonogenic growth defects in the hUCP2-silenced Patu8988T^{NI} cells (Fig. 4a and Extended Data Fig. 6a). Cells expressing mUcp2 had significantly lower ROS levels than those found in UCP2-silenced cells and Ctr$_{shRNA}$-transfected cells (Fig. 4b and Extended Data Fig. 6b). Higher ROS production in UCP2-silenced cells was associated with GSH/GSSG and NADPH/NADP$^+$ ratios lower than those of Ctr$_{shRNA}$-transfected cells whereas mUcp2 expression rescued the ratios to those of the Ctr cells (Fig. 4c,d). This suggested that mUcp2 re-established redox homeostasis in UCP2-silenced cells.

To confirm that doxycycline was not impacting respiration or altering redox homeostasis, we tested constitutively UCP2-silenced Patu8988T^{NI} cells. Our results confirmed that the lower GSH/GSSG and NADPH/NADP$^+$ ratios and OCRs in the presence of Gln were independent of doxycycline (Extended Data Fig. 6c–e). In this system, mUcp2 expression restored the cytosolic and organelle distribution of the [U-^{13}C]Gln-derived metabolites of UCP2-silenced Patu8988T^{NI} to Ctr levels (Extended Data Fig. 6f). This suggested that control of redox homeostasis by mUcp2 expression occurred through the proper functioning of *KRAS*-rewired Gln metabolism.

These results were validated in the xenograft model. In this case, doxycycline was administrated to mice 2 d after cell implantation. mUcp2 expression restored the proliferation rate of the hUCP2-silenced Patu8988T^{NI} cells, significantly increasing tumour mass (Fig. 4e and Extended Data Fig. 6g–i). UCP2 re-expression also restored the GSH/GSSG and NADPH/NADP$^+$ ratios found in UCP2-silenced Patu8988T^{NI}-derived tumours to those found in Ctrs (Fig. 4f,g). Collectively these data demonstrate that the observed differences in the two *KRAS*^{mut} PDAC cell lines were dependent on the expression of UCP2.

To verify the existence of any direct causal link between the acquisition of *KRAS* mutation and dependence on UCP2, we expressed the *KRAS*^{G12V} mutant, carried by the Patu8988T cells, in BxPC3 cells. *KRAS*^{G12V} expression (Extended Data Fig. 7a) did not alter the expression of UCP2 at the transcript or protein level (Extended Data Fig. 7b,c). Interestingly, *KRAS*^{G12V} increased the proliferation rate and clonogenic capacity of BxPC3 cells in a UCP2-dependent manner (Fig. 4h,i). These findings indicate that *KRAS* mutations do not regulate UCP2 expression; however, its biochemical function is crucial to support the increase of cell proliferation induced by mutated *KRAS*.

Together, these results demonstrate that the unknown mitochondrial transporter, which catalyses mitochondrial aspartate efflux in *KRAS*-rewired Gln metabolism[2], is UCP2 (Fig. 1a). We demonstrate in an in vivo model that UCP2 acts as a metabolite transporter like all other mitochondrial carrier family members[28]. Additionally, we show that the role UCP2 plays in ROS handling is linked to its substrate transport function rather than an uncoupling activity. Moreover, increased mitochondrial phosphate concentration produced by UCP2-dependent exchange reactions[9] would activate phosphate-dependent GLS[29] (Fig. 1a). It should be noted

that Mal, a reaction product of mitochondrial Gln oxidation and used by the cytosolic malic enzyme to generate NADPH[4,5], is efficiently exported by UCP2 in exchange for phosphate plus a proton[9]. In brief, the results reported above together with the Gln addiction found in many cancer cells, the increased expression of UCP2 in many tumours[30] and UCP2's tight regulation by Gln[10] make UCP2 an important metabolic target in PDAC and other Gln-dependent cancers.

Methods

Cell cultures. The cell lines Patu8988T (ACC-162), Panc1 (CRL-1469) and BxPC3 (CRL-1687) were sourced from ATCC and the KP2 (JCRB0181) cell line was sourced from the Japanese Collection of Research Bioresources Cell Bank. Although an unverified heterozygous mutation (c.34G>C, p.G12R) is reported in the Catalogue of Somatic Mutations in Cancer (COSMIC) database (https://cancer.sanger.ac.uk/cell_lines/sample/overview?id=1298218) for KP-2 cells, we used this cell line as the second *KRAS*^{WT} Ctr since, at the transcript level, we found an allelic imbalance in favour of the wild-type (WT) allele in these cells, as shown in two examples of forward and reverse sequences of PCR fragments (amplified from a first-strand complementary DNA) carried out in the study (Extended Data Fig. 8). Furthermore, based on previously published results[31], we estimate that less than 20% of the pancreatic KP-2 cell line population contained the mutated *KRAS* variant.

Cells were cultured continuously in 100 U ml^{-1} penicillin/streptomycin (catalogue no. ECB3001D; EuroClone), routinely checked for *Mycoplasma* contamination and used before passage 20–25. Roswell Park Memorial Institute 1640 (RPMI 1640) (catalogue no. ECB9006L) and DMEM (catalogue no. ECB7501L) medium, tetracycline-negative FCS (catalogue no. ECS0182L), dialysed FCS (HyClone, catalogue no. SH30079.03), Gln (catalogue no. ECB3000D) and glucose (catalogue no. 22700.01) were purchased from Euroclone. GSH reduced ethyl ester (catalogue no. G1404), *N*-acetyl-L-cysteine (catalogue no. A7250), doxycycline hyclate (catalogue no. D9891) and D-5030 medium (D5030) without glucose, L-glutamine, sodium pyruvate and non-essential amino acids were obtained from Sigma-Aldrich. Cells were cultured in the following media (specific growth media): Patu8988T and Panc1 in DMEM; and BxPC3 and KP-2 in RPMI 1640. All media were supplemented with 10% FCS, 10 mM of glucose and 2 mM of Gln. To check the effects of UCP2 silencing on PDAC cells, specific growth media and FCS were replaced with D5030 medium and dialysed FCS.

Lentiviral plasmids. The Tet-pLKO-puro-Scrambled plasmid, used as non-targeting shRNA (shCtr) in the inducible silencing experiments, was obtained from Addgene (plasmid no. 47541) (ref. [32]). The pLKO-puro-Scrambled plasmid, used in the non-inducible silencing experiments, was obtained from Addgene (plasmid no. 1864) (ref. [33]). The sequences of the two UCP2 silencing shRNAs are as follows: GTTCCTCTATCTCGTCTTG[9] (shRNA1) and CGGCCTGTATGATTCTGTCAA (TRCN0000060145) (shRNA2). shRNA1 and shRNA2 were cloned as AgeI/XbaI in the Tet-pLKO-puro (plasmid no. 21915; Addgene)[34] (inducible silencing) and, in shRNA1 only, in the pLKO-puro-Scrambled plasmid by replacing the shCtr sequence (non-inducible silencing). For mUcp2 expression, the coding sequence was cloned as NheI/MluI in the inducible expression plasmid pCW57-MCS1-P2A-MCS2 (Blast) (plasmid no. 80921; Addgene)[35]. Recombinant lentiviral particles were produced by transient transfection of 293T cells following a standard protocol. For the rescue experiments, Patu8988T cells were first transfected with the Ctr_pLKO.1 and shRNA1_pLKO.1 lentiviral particles and selected on puromycin (ant-pr-1; InvivoGen). Once the efficiency of silencing was checked, Ctr cells were transfected with the pCW57 empty vector (pCW57^{EV}) and shRNA1 cells were transfected with pCW57^{EV} or pCW57^{mUcp2} and selected on blasticidin (ant-bl-05; InvivoGen). The lentiviral plasmids used to express *KRAS*^{G12V} in BxPC3 cells were the two pLKO.1 vectors used in the rescue experiments. Briefly, in the BamHI- and KpnI-digested Ctr_pLKO.1 and shRNA1_pLKO.1 plasmids, we replaced the puromycin with the blasticidin resistance gene (*BSD*) amplified by PCR using pCW57-MCS1-P2A-MCS2 (Blast) as the template. The forward primer carried a BglII restriction site, compatible with the BamHI site, whereas the reverse primer carried BamHI and KpnI restriction sites downstream of the stop codon of the *BSD* (Extended Data Fig. 9a,b). The *KRAS*^{G12V} coding sequence was amplified by PCR using a first-strand cDNA derived from Patu8988T cell mRNA as the template. The forward primer carried an HA-Tag upstream of the starting methionine of *KRAS*. The PCR fragment, carrying XbaI and SalI restriction sites at the 5′ and 3′ ends, respectively, was cloned in the pULTRA plasmid (plasmid no. 24129; Addgene)[36], in frame with enhanced green fluorescent protein (eGFP) and a 'self-cleaving' P2A peptide sequences. Once we verified the sequences of all plasmids, the pULTRA plasmid was digested with BglII and KpnI, obtaining the KRAS expression cassette made up of the human ubiquitin C promoter, which controlled the EGFP-P2A-*KRAS*^{G12V} module and the woodchuck hepatitis virus post-transcriptional regulatory element sequence at the 3′ end. The expression cassette was cloned in the Ctr_pLKO.1 (Blast) and shRNA1_pLKO.1 (Blast) plasmids digested with BamHI and KpnI, downstream of *BSD* (Extended Data Fig. 9c,d). In this way, we constructed two all-in-one lentiviral plasmids expressing *KRAS*^{G12V} as well as the scramble or the shRNA1 RNA. Lentiviral particle production and cell transfection were carried out as reported above.

Yeast studies. The yeast strain used in all experiments was W303 (*MATa leu2-3,112 trp1-1 can1-100 ura3-1 ade2-1 his3-11,15*). The yeast gene deletions were constructed using the PCR-mediated gene disruption technique[37]. The hUCP2 and hUCP2R279Q open reading frames were cloned as HindIII/XhoI in the yeast expression vector pYES2 where the inducible *GAL1* promoter had been replaced with the constitutive *TDH3* promoter. Both proteins carried a V5-tag at their C termini. The endogenously deleted yeast genes *AGC1*, *AAT1*, *YMC2* and *ODC1* were cloned in the centromeric vector pRS416 whereas the *ODC2* gene was cloned in the pRS415 vector and used to verify the growth defect phenotype in oleate. For the initial propagation, yeast cells were grown in rich YP medium containing 2% Bacto Peptone and 1% yeast extract, supplemented with 2% glucose. The final pH was adjusted to 4.5. Growth in oleate was carried out by replacing the glucose with 0.5 mM of oleate (catalogue no. O1008; Sigma-Aldrich) dissolved in TERGITOL (catalogue no. 15S9; Sigma-Aldrich)[21].

Quantitative PCR with reverse transcription (qRT–PCR). Total RNA was extracted using the Blood/Tissue Total RNA Extraction Mini kit (Fisher Molecular Biology) according to the manufacturer's protocol. The first-strand cDNA was synthesized using the PrimeScript RT Master Mix Kit (catalogue no. RR036B; Takara). The quantitative PCR (qPCR) reactions were performed using an ABI Prism 7900 HT Real Time PCR system (Applied Biosystems). The TaqMan MGB assays for UCP1 (ID: Hs00222453_m1), UCP2 (ID: Hs01075227_m1), UCP3 (ID: Hs01106052_m1), UCP4 (ID: Hs00188687_m1), UCP5 (ID: Hs01073976_m1) and PPIA (ID: Hs04194521_s1) were purchased from Thermo Fisher Scientific. To quantify mUcp2, the qPCR was performed using the SYBR Select Master Mix (Applied Biosystems). The primers based on the cDNA sequences of the investigated genes were designed with Primer Express v.3.0 (Thermo Fisher Scientific) and purchased from Invitrogen (Thermo Fisher Scientific). The gene primer sequences used in the qPCR analyses were as follows: PPIA forward 5′-CATACGGGTCCTGGCATCTT-3′ and PPIA reverse 5′-TCCATGGCCTCCACAATATTC-3′; hUCP2 forward 5′-CACCTTTCCTCTGGATACTGCTAAA-3′ and hUCP2 reverse 5′-CACTGGCCCCTGACTTTCTC-3′; mUcp2 forward 5′-TCATCACTTTCCCTCTGGATACC-3′ and mUcp2 reverse 5′-GCGCACTAGCCCTTGACTCT-3′.

The specificity of the PCR amplification was checked with the heat dissociation protocol after the final cycle of PCR. To correct for differences in the amount of starting first-strand cDNA, the human *PPIA* gene was amplified in parallel as a reference gene[38]. Fluorescence data were calculated using the SDS software v.2.4 (Applied Biosystems). The relative quantification of mRNA for the UCPs genes was performed according to the comparative method ($2^{-\Delta\Delta C_T}$), where the ΔC_T sample is the C_T sample − C_T reference gene, and C_T is the threshold cycle[39]. For each silenced cell line, the value of $2^{-\Delta\Delta C_T}$ indicates the fold change in mRNA values relative to the ΔC_T of the control cell line (calibrator). For the analyses, reverse-transcribed cDNA from three biological replicates was used and three technical replicates were analysed for each biological replicate. The following doxycycline concentrations were used for UCP2 silencing: 500 ng ml^{-1} (Patu8988T and Panc1); 250 ng ml^{-1} (BxPC3); and 100 ng ml^{-1} (KP-2); 500 ng ml^{-1} was used for the induction of mUcp2 in Patu8988T^{NI}.

Western blot analysis. PDAC cell lysates (approximately 100 µg of proteins) were separated by SDS–polyacrylamide gel electrophoresis and transferred onto nitrocellulose membrane by a Trans-Blot Turbo Transfer System (Bio-Rad Laboratories). Samples were not heated before loading. Membranes were blocked in Tris-buffered saline (TBS) containing 1% BSA and 0.1% Tween 20, before incubation with the primary antibody overnight at 4 °C. Membranes were washed with TBS and Tween 20 and incubated with the appropriate dilution of the horseradish peroxidase (HRP)-conjugated secondary antibody for 1 h at room temperature and washed again. Immunoblotting on yeast cells was carried out as stated above and cell lysates were prepared as described previously[40]. Briefly, yeast cells were resuspended in 100 µl of distilled water and 100 µl of 0.2 M NaOH, incubated for 5 min at room temperature and centrifuged at 12,000 r.p.m. The pellet was resuspended in 50 µl SDS sample buffer and boiled for 3 min before loading. V5-tagged UCP2 and UCP2^{R279Q} were detected with an anti-V5 monoclonal antiserum. A rabbit antiserum against yeast porin[41], a kind gift from L. Pelosi, was used for protein normalization. The SuperSignal West Pico PLUS Chemiluminescent Substrate (no. 34577; Thermo Fisher Scientific) was used to immunodecorate UCP2 and a standard ECL kit (Pierce) was used for COX4, HA-tagged *KRAS*^{G12V}, V5-tagged UCP2, yeast porin and AGC1/2. Protein-specific signals were detected densitometrically—5 min of acquisition for UCP2 and few seconds for COX4, HA-tagged *KRAS*^{G12V}, V5-tagged UCP2, yeast porin and AGC1/2. The following antibodies were used: anti-UCP2 (murine custom-made antibody, 1:20,000); anti-AGC1/2 (rabbit custom-made antibody, 1:5,000); anti-HA (anti-HA.11 epitope, clone 16B12, 1:5,000: BioLegend); anti-V5-Tag (1:5,000;

catalogue no. 13202; Cell Signaling Technology); anti-COX4 (F-8, 1:5,000; catalogue no. sc-376731, Santa Cruz Biotechnology); and anti-yeast porin (rabbit custom-made antibody, 1:5,000). The following secondary antibodies were used: a goat anti-mouse IgG (H+L) secondary antibody, HRP (catalogue no. 31430; Thermo Fisher Scientific) 1:50,000 (UCP2), 1:10,000 (HA-tagged *KRAS*^{G12V}), 1:20,000 (COX4); and a goat anti-rabbit IgG (H+L) secondary antibody, HRP (catalogue no. 31460; Thermo Fisher Scientific) 1:10,000 (V5-tagged UCP2), 1:10,000 (AGC1/AGC2) and 1:10,000 (yeast porin).

Transport assays. Mitochondria were isolated from the PDAC cell lines using a mitochondrial isolation kit for cultured cells (catalogue no. 89874; Thermo Fisher Scientific) with the Halt Protease Inhibitor Mixture (catalogue no. 78415; Thermo Fisher Scientific) according to the manufacturer's instructions; 100 µg of isolated mitochondria was solubilized for 45 min on ice in a buffer containing 2% Triton X-114 (catalogue no. X-114; 500 ml; Sigma-Aldrich), 1 mM of EDTA, 10 mM of PIPES, pH 7.4 and cardiolipin (4 mg ml^{-1} final concentration) (catalogue no. C0563; Sigma-Aldrich) and centrifuged at 13,800*g* for 15 min at 4 °C. Triton-solubilized proteins were immediately incorporated into phospholipid vesicles by cyclic removal of the detergent using a hydrophobic column (Amberlite, catalogue no. 152-3920; Bio-Rad Laboratories)[42]. The composition of the initial mixture used for reconstitution was 90 µl of Triton-solubilized extract, 70 µl of Triton X-114 (10% w/v), 110 µl of L-α-phosphatidylcholine from egg yolk (10% w/v) (catalogue no. 61771; Sigma-Aldrich) in the form of sonicated liposomes, 20 mM of P_i or 10 mM of ATP (catalogue no. A2383; Sigma-Aldrich), 10 mM of PIPES (pH 7.0), 0.8 mg ml^{-1} cardiolipin and water to a final volume of 700 µl.

Transport was started by adding [^{14}C]Asp (1 mM) (MC-139; Moravek) or [^{14}C]ADP (50 µM) (NEC559050UC; PerkinElmer) outside the proteoliposomes and stopped after 30 min with a mixture of pyridoxal 5′-phosphate monohydrate (10 mM; catalogue no. 82870; Sigma-Aldrich) and bathophenanthrolinedisulfonic acid disodium salt hydrate (10 mM) (catalogue no. 146617; Sigma-Aldrich). All reconstitution and transport assay steps were carried out at 25 °C at the same internal and external pH value (pH 7.0). Finally, external radioactivity was removed from each sample of proteoliposomes by a Sephadex G-75 superfine column (catalogue no. GE17-0051-01; GE Healthcare); proteoliposomes were eluted with 50 mM of NAC and their radioactivity was measured[43]. The reconstitution and transport assays of the bacterially expressed UCP2 and UCP2^{R279Q} were carried as described above and reported previously[9].

Cell proliferation and clonogenic assays. An appropriate number of cells was seeded in 6× multi-well plates in the specific growth media with doxycycline (500 ng ml^{-1} (Patu8988T and Panc1 cells), 250 ng ml^{-1} (BxPC3 cells) and 100 ng ml^{-1} (KP-2 cells)). The next day, media were changed with D5030 supplemented with 2 mM of Gln, 10 mM of glucose, 10% dialysed FCS and doxycycline. In some experiments, 2 mM of Asp, 1 mM of Glu, 4 mM of glutathione reduced ethyl ester or 4 mM of NAC were added. Medium was not substituted during the experiment even though similar results were obtained by changing the medium every 2 d. The proliferation rate was regularly determined from days 1 to 9. Cells were counted by an automated Scepter Counter Cells (proliferation assay). After 2–3 weeks, colonies were gently washed with PBS without calcium and magnesium (catalogue no. BE17-516F; Lonza), fixed in 80% methanol and stained with 0.5% crystal violet. After image acquisition, colonies were counted (clonogenic assay).

GSH/GSSG and NADP$^+$/NADPH assays. A total of 2×10^6 to 4×10^6 PDAC cells grown in D5030, and 30–60 mg of frozen tumours were assayed. NADPH / NADP$^+$ ratios were determined using the NADPH/NADP$^+$ assay kit (catalogue no. K347; BioVision) according to the manufacturer's instructions. After cell lysis, the NADPH/NADP$^+$ inhibiting enzymes were removed using a 10 kDa spin column (Vivaspin 500, catalogue no. GE28-9322-25; Sigma-Aldrich). The GSH/GSSG ratios were determined using the Glutathione Fluorescent Detection Kit (catalogue no. EIAGSHF; Thermo Fisher Scientific) according to the manufacturer's instructions. In both assays, the concentration was obtained by comparison to standard curves.

Measurement of total ROS. The four human PDAC cell lines were plated in specific growth media with doxycycline. The next day, the medium was changed to D5030 medium supplemented with 2 mM of Gln, 10 mM of glucose, 10% dialysed FCS and doxycycline. After 4 d, 2×10^5 cells per sample were stained with 10 µM 2′,7′-dichlorodihydrofluorescein diacetate (H2DCFDA; Molecular Probes) for 30 min at 37 °C. After staining, cells were washed and measured using an Attune NxT Acoustic Focusing Cytometer (Thermo Fisher Scientific). Analysis was performed and data visualized using the Attune NxT software v.2.6.

OCR. PDAC cells (Patu8988T and BxPC3) were plated into XF Cell Culture Microplates (Seahorse BioScience) in specific growth media with doxycycline and incubated overnight at 37 °C and 5% CO_2. The next day, the medium was replaced with D5030 supplemented with 2 mM of Gln, 10 mM of glucose, 10% dialysed FCS and doxycycline, pH 7.4. On the third day, to measure the OCR, the medium was replaced with the Seahorse XF base medium (catalogue no. 103193-100; Agilent), supplemented with 2 mM of Gln and the plate was incubated at 37 °C without CO_2 for 1 h. During the experiment, 2 µM of oligomycin (catalogue no. 04876; Sigma-Aldrich), 0.5 µM of FCCP (catalogue no. C2759; Sigma-Aldrich) and 1 µM of antimycin A (catalogue no. A8674; Sigma-Aldrich) + 1 µM of rotenone (catalogue no. R8875; Sigma-Aldrich) were sequentially injected. The experiments were run using a Seahorse XFe96 Analyzer (Agilent) and data analysis was carried out with the Wave Desktop software v.2.2. The raw data were normalized to the total protein amount per well measured at the end of the experiment.

UCP2 expression analysis in PDAC and GSEA. Transcript abundance of UCP2 from PDAC primary tumour samples, normal pancreatic tissues and PDAC cell lines was determined by analysing the GEPs of different publicly available datasets[44–49]. All GEPs (HG-U133_Plus 2.0 and HG_U219 arrays from the Affymetrix platform) were processed by using the robust multi-array average normalization method by means of RMAExpress v.1.2.0. Probes were then collapsed to unique genes by selecting the ones with the maximal average expression for each gene and the expression values were $\log_2$-transformed. The difference of UCP2 expression between PDAC samples and normal pancreas was determined by Mann–Whitney *U*-test with the R statistical programming environment v.3.4.3. The source data used to perform the UCP2 expression analysis in PDAC primary tumour samples and cell lines are reported in Supplementary Table 2. GSEA[50] was performed on publicly available PDAC datasets[46,51] by using continuous UCP2 expression level to label tumour samples. Genes were ranked by the Pearson metric method. We then tested roughly 200 gene sets related to different metabolic pathways gathered from the MSigDB collection (https://www.gsea-msigdb.org/gsea/msigdb/collections.jsp).

Stable isotope analysis using gas chromatography–mass spectrometry (GC–MS). *Rapid subcellular fractionation and metabolite extraction.* Doxycycline-induced PDAC cells were cultured in 6-well plates in D5030 medium supplemented with 10 mM of glucose, 10% dialysed FCS plates and 2 mM of [U-^{13}C]Gln for 24 h. Cytosolic and mitochondrial-enriched pool separation was carried out as described previously[20] with some modifications, that is, digitonin (D5628; Sigma-Aldrich) cell permeabilization was carried out on adherent cells and the amount of digitonin used was much lower. Briefly, after tracer incubation, the 6-well plate was placed on ice and cells were washed twice with ice-cold PBS, then they were incubated for 2 min with 300 µl of a buffer containing NaCl (150 mM), $MgCl_2$ (5 mM), $KHCO_3$ (20 mM), pH 7.4, and digitonin (Patu8988T (100 µg) and BxPC3 (200 µg) per million of cells). The supernatant (cytosolic fraction) was removed and immediately quenched in 1 ml of methanol/chloroform (1:1, −20 °C). Permeabilized cells were washed once with the permeabilization buffer without digitonin, quenched with 500 µl of methanol (−60 °C), scraped from the well and collected in a tube containing 800 µl of chloroform/water (1.67:1) (mitochondrial-enriched fraction). The two fractions were vortexed for 5 min at 4 °C and centrifuged at 14,000 r.p.m. for 10 min at 4 °C; the upper phase recovered, dried using a SpeedVac and stored at −80 °C until derivatization. During metabolite extraction, tartaric acid was used as the internal standard to normalize the efficiency of derivatization. The integrity of mitochondria in the permeabilization buffer was checked by: (1) respirometry, using the correct number of cells per amount of digitonin ratio, PDAC cells and efficiently respired succinate and respiration was inhibited by oligomycin and uncoupled by FCCP; (2) PDAC cells transfected with a mitochondria-targeted GFP[52] and treated with the permeabilization buffer did not release any fluorescence from the mitochondria after 4 min of treatment (Extended Data Fig. 3m). Similar results were obtained if digitonin was replaced by 10 nM of recombinant PFO (XF PMP)[53]. Images were acquired with a ×63 plan apo objective every 20 s with an exposure time of 100 ms (MetaMorph software v.6.1).

Derivatization. Dried sample were dissolved in 50 µl of methoxamine reagent (Sigma-Aldrich) and sonicated for 10 min. Samples were then kept at 40 °C for 90 min, then at 70 °C for 30 min after the addition of 70 µl of MTBSTFA + 1% TBDMCS (Thermo Fisher Scientific)[54]. Samples were next transferred to vials equipped with inserts.

GC–MS measurements. A Waters Micromass Quattro Micro GC triple quadrupole mass spectrometer, directly interfaced to an Agilent 6890N gas chromatograph was used to analyse the samples. Samples (2 µl) were injected in splitless mode into the gas chromatograph and then separated with a fused silica DB-5MS + DG capillary column (30 m, 0.25 mm inside diameter, 0.25 µm thickness of the inner liquid in the column). The injector temperature was set to 240 °C. High purity helium was used as the carrier gas at a constant flow rate of 1 ml min^{-1}. The column temperature was initially kept at 70 °C for 2 min, ramped up to 140 °C at 3 °C min^{-1}, ramped up to 150 °C at 1 °C min^{-1} and ramped up to 280 °C at 3 °C min^{-1}. The interphase and ion source temperatures were 280 and 240 °C, respectively. Data were acquired in selected ion monitoring[54] mode and the integrated peak area of the targeted labelled ions was normalized by the peak area of tartrate. All metabolites were quantified using five-point external calibration curves over the range of 1–1,000 ng per metabolite. The quantity of metabolite fraction analysed was adjusted to the corresponding protein concentration calculated on processing

a parallel 6-well plate. Data were acquired and processed using the MassLynx software v.4.0.

Organotypic 3D culture. PDAC cells were seeded at an appropriate density in 96-well plates on top of an extracellular matrix gel prepared by Matrigel (Corning Matrigel Growth Factor Reduced Basement Membrane Matrix, Phenol Red-Free) with serum-free specific growth media, to a final concentration of 7 mg ml^{-1}. One hundred microlitres per well were plated into 96-well plates and incubated for 60 min in a 37 °C incubator allowing the gels to solidify. The next day, D5030 medium was added and growth was maintained for a total of 7 d, with a change of medium every 2 d. After 5 or 7 d under these growth conditions, colonies were photographed using the TE200 microscope (Nikon). Cell viability was measured using the Resazurin cell viability assay (Immunological Sciences). Resazurin (10 µl) was added to each 100 µl of medium according to the manufacturer's instructions and fluorescence was measured after approximately 3 h. Cell death was assayed by incubating the cells overnight at 37 °C with ethidium homodimer-1 (16 nM). The images with ethidium homodimer-1 were acquired with an ×4 air objective using a Nikon EclipseTi-S epifluorescence microscope and analysed for integrated density using ImageJ bundled with Java 1.8.0_172 (http://rsb.info.nih.gov/ij/).

Xenograft studies. For subcutaneous xenografts, 5-week-old female SCID mice (C.B-17/IcrHanHsd-Prkdc^{scid} congenic strain of BALB/cAnIcr) were purchased from ENVIGO RMS. Mice were housed under a 12-h light–dark cycle at 23 ± 1 °C and 50 ± 5% humidity; ad libitum diet and water were provided. Control, UCP2-silenced and rescued PDAC cells (Patu8988T (7×10^5), Panc1, BxPC3 and KP-2 ($1.5–2 \times 10^6$)) suspended in 200 µl of Hanks' buffered saline solution, were injected subcutaneously into the interscapular region of each mouse (5 animals per group). Tumour length and width were measured with a calliper and the volume was calculated according to the following formula: (length × width^2)/2. No littermate controls were used. When tumour sizes reached a 40–70 mm^3 volume, animals were given doxycycline water (doxycycline 2 g l^{-1}, sucrose 20 g l^{-1}). For the rescue experiment, doxycycline water was administered 2 d after the injection. Tumour volume was measured once per week. For 3 out of 60 mice used in the xenograft experiments, the final tumour volume exceeded approximately 10% the maximal tumour volume (2 cm^3) established by our animal care committee for implanted tumours in the interscapular region (Extended Data Figs. 5c and 6g). All tumour-bearing animals, for all the duration of the experiment, were observed daily to screen for behavioural changes resulting from tumour burden. All end points established by our animal care committee were complied with as follows: (1) absence of tumour ulceration; (2) parental care; (3) food and water intake; (4) no loss of body weight; (5) no locomotion limitation; (6) no cachexia. No animal presented any of these end points for the duration of the experiment. At the end of each experiment, animals were euthanized and the xenografts were collected and subjected to downstream end point analysis. All xenograft experiments with human PDAC lines were approved by the Italian Ministry of Health under protocol no. 418/2015-PR. All animals were maintained and handled in accordance with the recommendation of the Guidelines for the Care and Use of Laboratory Animals and experiments were approved by the Animal Care Committee of University of Calabria, Italy.

Immunohistochemical analysis. Tumours were fixed in 4% formalin, embedded in paraffin and sectioned (5 µm). The sections were mounted on slides precoated with poly-lysine and then deparaffinized and dehydrated (7–8 serial sections). The immunohistochemical experiments were performed after heat-mediated antigen retrieval using human Ki67 (1:100 clone MIB-1; DAKO) primary antibodies at 4 °C overnight. Then, a biotinylated specific IgG was applied for 1 h at room temperature, followed by avidin–biotin HRP complex (VECTASTAIN ABC Kit; Vector Laboratories). Immunoreactivity was visualized using DAB Peroxidase (HRP) Substrate Kit, 3,3′-diaminobenzidine (Vector Laboratories). The immunostained slides of tumour samples were evaluated by light microscopy using ×20 magnification (Olympus BX51 microscope).

Scoring system. Six to seven serial sections were scored in a blinded manner for each sample by two independent observers. To quantify the proliferation index, the percentage of Ki-67$^+$ cells was counted in 10 random fields at ×20 magnification (Olympus BX51 microscope).

Statistical analysis. Prism 7 (GraphPad Software) was used to conduct the statistical analysis of all data, except for the qPCR and Seahorse data where Microsoft Excel v.16.40 was used. Data are presented as the mean ± s.d. All quantitative results were assessed by unpaired, two-tailed Student's *t*-test or Mann–Whitney *U*-test after confirming that the data met the appropriate assumptions. The Student's *t*-test assumed two-tailed distributions to calculate statistical significance between groups. Unless otherwise indicated, for all in vitro experiments, two independent experiments with three replicates were analysed. For the mouse studies, tumour development and staining intensity of tissue sections were scored in a blinded manner. GC–MS studies were also carried out in a blinded manner. $P < 0.05$ was considered statistically significant and *P* values are indicated in the figures.

Reporting Summary. Further information on research design is available in the Nature Research Reporting Summary linked to this article.

Data availability

All data used for the expression analysis and GSEA are publicly available. The datasets using HG133plus2 from Affymetrix included ArrayExpress accession no. E-MEXP-2780 and Gene Expression Omnibus accession nos. GSE15471, GSE22780, GSE16515, GSE32676, GSE42952 and GSE36133. The dataset using HG_U219 from Affymetrix included ArrayExpress accession no. E-MTAB-6134. The unverified heterozygous mutation (c.34G>C, p.G12R) for KP-2 cells is reported in the COSMIC with sample ID COSS1298218. There are no restrictions on data availability. Any additional information supporting the data associated with this paper and the findings of this study is available from the corresponding authors upon request. Source data are provided with this paper.

Received: 14 September 2019; Accepted: 22 October 2020;
Published online: 23 November 2020

References

1. Ying, H. et al. Oncogenic Kras maintains pancreatic tumors through regulation of anabolic glucose metabolism. *Cell* **149**, 656–670 (2012).
2. Son, J. et al. Glutamine supports pancreatic cancer growth through a KRAS-regulated metabolic pathway. *Nature* **496**, 101–105 (2013).
3. Hensley, C. T., Wasti, A. T. & DeBerardinis, R. J. Glutamine and cancer: cell biology, physiology, and clinical opportunities. *J. Clin. Invest.* **123**, 3678–3684 (2013).
4. Altman, B. J., Stine, Z. E. & Dang, C. V. From Krebs to clinic: glutamine metabolism to cancer therapy. *Nat. Rev. Cancer* **16**, 619–634 (2016).
5. DeBerardinis, R. J. et al. Beyond aerobic glycolysis: transformed cells can engage in glutamine metabolism that exceeds the requirement for protein and nucleotide synthesis. *Proc. Natl Acad. Sci. USA* **104**, 19345–19350 (2007).
6. Abrego, J. et al. *GOT1*-mediated anaplerotic glutamine metabolism regulates chronic acidosis stress in pancreatic cancer cells. *Cancer Lett.* **400**, 37–46 (2017).
7. Chakrabarti, G. et al. Targeting glutamine metabolism sensitizes pancreatic cancer to PARP-driven metabolic catastrophe induced by β-lapachone. *Cancer Metab.* **3**, 12 (2015).
8. Wang, Y.-P. et al. Arginine methylation of MDH1 by CARM1 inhibits glutamine metabolism and suppresses pancreatic cancer. *Mol. Cell* **64**, 673–687 (2016).
9. Vozza, A. et al. UCP2 transports C4 metabolites out of mitochondria, regulating glucose and glutamine oxidation. *Proc. Natl Acad. Sci. USA* **111**, 960–965 (2014).
10. Pecqueur, C. et al. Uncoupling protein 2, in vivo distribution, induction upon oxidative stress, and evidence for translational regulation. *J. Biol. Chem.* **276**, 8705–8712 (2001).
11. Rupprecht, A., Moldzio, R., Mödl, B. & Pohl, E. E. Glutamine regulates mitochondrial uncoupling protein 2 to promote glutaminolysis in neuroblastoma cells. *Biochim. Biophys. Acta, Bioenerg.* **1860**, 391–401 (2019).
12. Nübel, T. et al. Modified glutamine catabolism in macrophages of *Ucp2* knock-out mice. *Biochim. Biophys. Acta* **1777**, 48–54 (2008).
13. Donadelli, M., Dando, I., Fiorini, C. & Palmieri, M. UCP2, a mitochondrial protein regulated at multiple levels. *Cell. Mol. Life Sci.* **71**, 1171–1190 (2014).
14. Bouillaud, F., Couplan, E., Pecqueur, C. & Ricquier, D. Homologues of the uncoupling protein from brown adipose tissue (UCP1): UCP2, UCP3, BMCP1 and UCP4. *Biochim. Biophys. Acta* **1504**, 107–119 (2001).
15. Palmieri, L. et al. Citrin and aralar1 are Ca^{2+}-stimulated aspartate/glutamate transporters in mitochondria. *EMBO J.* **20**, 5060–5069 (2001).
16. Owen, O. E., Kalhan, S. C. & Hanson, R. W. The key role of anaplerosis and cataplerosis for citric acid cycle function. *J. Biol. Chem.* **277**, 30409–30412 (2002).
17. Alkan, H. F. et al. Cytosolic aspartate availability determines cell survival when glutamine is limiting. *Cell Metab.* **28**, 706–720.e6 (2018).
18. Yoo, H. C. et al. A variant of SLC1A5 is a mitochondrial glutamine transporter for metabolic reprogramming in cancer cells. *Cell Metab.* **31**, 267–283.e12 (2020).
19. Dalla Pozza, E. et al. Role of mitochondrial uncoupling protein 2 in cancer cell resistance to gemcitabine. *Biochim. Biophys. Acta* **1823**, 1856–1863 (2012).
20. Lee, W. D., Mukha, D., Aizenshtein, E. & Shlomi, T. Spatial-fluxomics provides a subcellular-compartmentalized view of reductive glutamine metabolism in cancer cells. *Nat. Commun.* **10**, 1351 (2019).
21. Cavero, S. et al. Identification and metabolic role of the mitochondrial aspartate-glutamate transporter in *Saccharomyces cerevisiae*. *Mol. Microbiol.* **50**, 1257–1269 (2003).
22. Porcelli, V. et al. Molecular identification and functional characterization of a novel glutamate transporter in yeast and plant mitochondria. *Biochim. Biophys. Acta Bioenerg.* **1859**, 1249–1258 (2018).

23. Palmieri, F. Mitochondrial transporters of the SLC25 family and associated diseases: a review. *J. Inherit. Metab. Dis.* **37**, 565–575 (2014).
24. Monné, M., Miniero, D. V., Iacobazzi, V., Bisaccia, F. & Fiermonte, G. The mitochondrial oxoglutarate carrier: from identification to mechanism. *J. Bioenerg. Biomembr.* **45**, 1–13 (2013).
25. Tessa, A. et al. Identification of novel mutations in the *SLC25A15* gene in hyperornithinemia-hyperammonemia-homocitrullinuria (HHH) syndrome: a clinical, molecular, and functional study. *Hum. Mutat.* **30**, 741–748 (2009).
26. Fiermonte, G. et al. An adult with type 2 citrullinemia presenting in Europe. *N. Engl. J. Med.* **358**, 1408–1409 (2008).
27. Palmieri, L. et al. Identification in *Saccharomyces cerevisiae* of two isoforms of a novel mitochondrial transporter for 2-oxoadipate and 2-oxoglutarate. *J. Biol. Chem.* **276**, 1916–1922 (2001).
28. Palmieri, F. The mitochondrial transporter family (SLC25): physiological and pathological implications. *Pflugers Arch.* **447**, 689–709 (2004).
29. Cassago, A. et al. Mitochondrial localization and structure-based phosphate activation mechanism of Glutaminase C with implications for cancer metabolism. *Proc. Natl Acad. Sci. USA* **109**, 1092–1097 (2012).
30. Baffy, G. Uncoupling protein-2 and cancer. *Mitochondrion* **10**, 243–252 (2010).
31. Gao, J. et al. Validation of targeted next-generation sequencing for *RAS* mutation detection in FFPE colorectal cancer tissues: comparison with Sanger sequencing and ARMS-Scorpion real-time PCR. *BMJ Open* **6**, e009532 (2016).
32. Rudin, C. M. et al. Comprehensive genomic analysis identifies *SOX2* as a frequently amplified gene in small-cell lung cancer. *Nat. Genet.* **44**, 1111–1116 (2012).
33. Sarbassov, D. D., Guertin, D. A., Ali, S. M. & Sabatini, D. M. Phosphorylation and regulation of Akt/PKB by the rictor-mTOR complex. *Science* **307**, 1098–1101 (2005).
34. Wiederschain, D. et al. Single-vector inducible lentiviral RNAi system for oncology target validation. *Cell Cycle* **8**, 498–504 (2009).
35. Barger, C. J., Branick, C. & Chee, L. & Karpf, A. R. Pan-cancer analyses reveal genomic features of *FOXM1* overexpression in cancer. *Cancers (Basel)* **11**, 251 (2019).
36. Lou, E. et al. Tunneling nanotubes provide a unique conduit for intercellular transfer of cellular contents in human malignant pleural mesothelioma. *PLoS ONE* **7**, e33093 (2012).
37. Wach, A. PCR-synthesis of marker cassettes with long flanking homology regions for gene disruptions in *S. cerevisiae*. *Yeast* **12**, 259–265 (1996).
38. Agrimi, G., Russo, A., Scarcia, P. & Palmieri, F. The human gene *SLC25A17* encodes a peroxisomal transporter of coenzyme A, FAD and NAD^+. *Biochem. J.* **443**, 241–247 (2012).
39. Bustin, S. A. Absolute quantification of mRNA using real-time reverse transcription polymerase chain reaction assays. *J. Mol. Endocrinol.* **25**, 169–193 (2000).
40. Kushnirov, V. V. Rapid and reliable protein extraction from yeast. *Yeast* **16**, 857–860 (2000).
41. De Marcos Lousa, C., Trézéguet, V., Dianoux, A.-C., Brandolin, G. & Lauquin, G. J. The human mitochondrial ADP/ATP carriers: kinetic properties and biogenesis of wild-type and mutant proteins in the yeast *S. cerevisiae*. *Biochemistry* **41**, 14412–14420 (2002).
42. Li, Y. et al. Functional characterization of the partially purified Sac1p independent adenine nucleotide transport system (ANTS) from yeast endoplasmic reticulum. *J. Biochem.* **164**, 313–322 (2018).
43. Vozza, A. et al. Biochemical characterization of a new mitochondrial transporter of dephosphocoenzyme A in *Drosophila melanogaster*. *Biochim. Biophys. Acta Bioenerg.* **1858**, 137–146 (2017).
44. Badea, L., Herlea, V., Dima, S. O., Dumitrascu, T. & Popescu, I. Combined gene expression analysis of whole-tissue and microdissected pancreatic ductal adenocarcinoma identifies genes specifically overexpressed in tumor epithelia. *Hepatogastroenterology* **55**, 2016–2027 (2008).
45. Pei, H. et al. FKBP51 affects cancer cell response to chemotherapy by negatively regulating Akt. *Cancer Cell* **16**, 259–266 (2009).
46. Barretina, J. et al. The Cancer Cell Line Encyclopedia enables predictive modelling of anticancer drug sensitivity. *Nature* **483**, 603–607 (2012).
47. Donahue, T. R. et al. Integrative survival-based molecular profiling of human pancreatic cancer. *Clin. Cancer Res.* **18**, 1352–1363 (2012).
48. Van den Broeck, A., Vankelecom, H., Van Eijsden, R., Govaere, O. & Topal, B. Molecular markers associated with outcome and metastasis in human pancreatic cancer. *J. Exp. Clin. Cancer Res.* **31**, 68 (2012).
49. Winter, C. et al. Google goes cancer: improving outcome prediction for cancer patients by network-based ranking of marker genes. *PLoS Comput. Biol.* **8**, e1002511 (2012).
50. Subramanian, A. et al. Gene set enrichment analysis: a knowledge-based approach for interpreting genome-wide expression profiles. *Proc. Natl Acad. Sci. USA* **102**, 15545–15550 (2005).
51. Puleo, F. et al. Stratification of pancreatic ductal adenocarcinomas based on tumor and microenvironment features. *Gastroenterology* **155**, 1999–2013.e3 (2018).
52. Marchi, S., Bonora, M., Patergnani, S., Giorgi, C. & Pinton, P. Methods to assess mitochondrial morphology in mammalian cells mounting autophagic or mitophagic responses. *Methods Enzymol.* **588**, 171–186 (2017).
53. Divakaruni, A. S. et al. Thiazolidinediones are acute, specific inhibitors of the mitochondrial pyruvate carrier. *Proc. Natl Acad. Sci. USA* **110**, 5422–5427 (2013).
54. Young, J. D., Allen, D. K. & Morgan, J. A. Isotopomer measurement techniques in metabolic flux analysis II: mass spectrometry. *Methods Mol. Biol.* **1083**, 85–108 (2014).

Acknowledgements

This work was supported by a grant from the Italian Association for Cancer Research (AIRC no. IG 2014 Id.15404 to G.F.) and a grant from the Italian Ministero dell'Istruzione, dell'Università e della Ricerca (no. 2017PAB8EM_002 to G.F.).

Author contributions

S.R., C.P., A.V., D.F. and L.C. performed most of the in vitro experiments. F.D. performed the in vitro reconstitution experiments. I.P. performed the cytofluorimetric analyses. S.N.B. and F.M.L. performed the respirometry experiments. R.G., G.E.D. and G.A. performed the GS–MS metabolomics experiments. P.S. carried out the RT–PCR experiments. Y.L., C.M.T.M. and F.P. performed the yeast experiments. V.R., R.M. and V.D. performed the xenograft experiments. M.R.G., R.A.C. and S.J.R. performed the organotypic cell culture experiments. M.C.V. performed the GSEA and analysis on GEP. L.P., V.D. and G.F. conceived and designed the study. W.S., L.P., V.D., E.M., C.L.R. and G.F. interpreted the results and wrote the manuscript. G.F. acquired the funding.

Competing interests

The authors declare no competing interests.

Additional information

Extended data is available for this paper at https://doi.org/10.1038/s42255-020-00315-1.

Supplementary information is available for this paper at https://doi.org/10.1038/s42255-020-00315-1.

Correspondence and requests for materials should be addressed to V.D. or G.F.

Peer review information Primary Handling Editors: Elena Bellafante; Christoph Schmitt. *Nature Metabolism* thanks the anonymous reviewers for their contribution to the peer review of this work.

Reprints and permissions information is available at www.nature.com/reprints.

Publisher's note Springer Nature remains neutral with regard to jurisdictional claims in published maps and institutional affiliations.

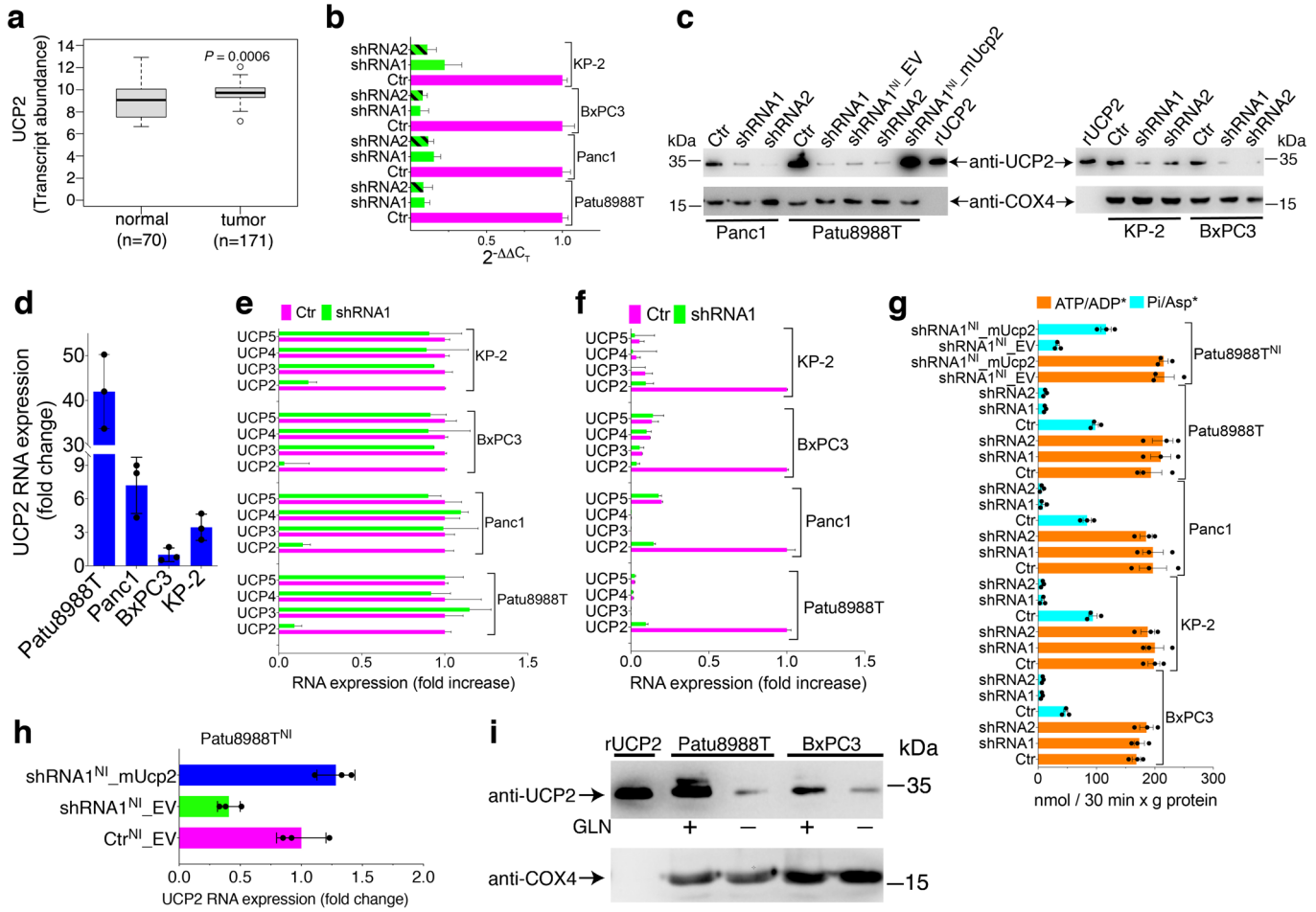

Extended Data Fig. 1 | Expression analysis of UCP2 and UCP2 homologs in PDAC cells. a, Transcript abundance of UCP2 in PDAC primary tumour samples and normal pancreatic tissues derived from gene expression profiling (GEP) of different publicly available datasets. **b**-**d**, The relative expression of *UCP2* in control and *UCP2*^{shRNA}-transfected PDAC cells. *UCP2* transcript levels were quantified by qPCR (**b** and **d**) and UCP2 protein levels were assayed with a UCP2-specific antiserum (**c**). An anti-COX4 antibody was used for normalization. **e, f**, UCP2 silencing does not alter the expression levels of other UCP homologs. The relative expression of all UCP genes was quantified by qPCR. The ΔC_T of the indicated UCP homolog gene (**e**) and that of UCP2 (**f**) of the Ctr^{shRNA}-transfected cells were used as internal calibrators. **g**, ATP/ADP and Pi/Asp exchanges activities catalysed by mitochondrial extracts of control, UCP2-silenced and UCP2-silenced rescued PDAC cells. Mitochondria were solubilized with detergent and reconstituted into liposomes containing Pi or ATP. The exchange reaction was started by adding [^{14}C]aspartate or [^{14}C]ADP to proteoliposomes and stopped after 30 minutes with inhibitors. Values represent means ± SD of three independent experiments. **h**, Expression of murine Ucp2 (mUcp2) gene in Patu8988T cells. The relative expression of human *UCP2* and murine Ucp2 were determined by Sybr green qPCR. The ΔC_T of human *UCP2* of the Ctr^{shRNA}-transfected cells carrying the empty expression vector (EV) was used as internal calibrator. The protein expression levels of panel **h** are shown in panel **c**. **i**, Effect of glutamine on UCP2 protein expression levels. The total cell extracts were assayed in the presence or absence (overnight starvation) of glutamine. For all transcript analyses, reverse transcribed cDNA from three biological replicates was used and three technical replicates were analysed for each biological replicate, values represent means ± SD (**b**, **d**-**f**, **h**). COX4 normalization was carried out on the same SDS-PAGE used to assay UCP2 expression levels, similar results were obtained in three biologically independent experiments (**c**, **i**). Statistical significance was calculated by unpaired two-tailed Mann–Whitney *U*-test (**a**). rUCP2, recombinant human UCP2. Patu8988T^{NI}, cells transfected with non-inducible lentiviral plasmids.

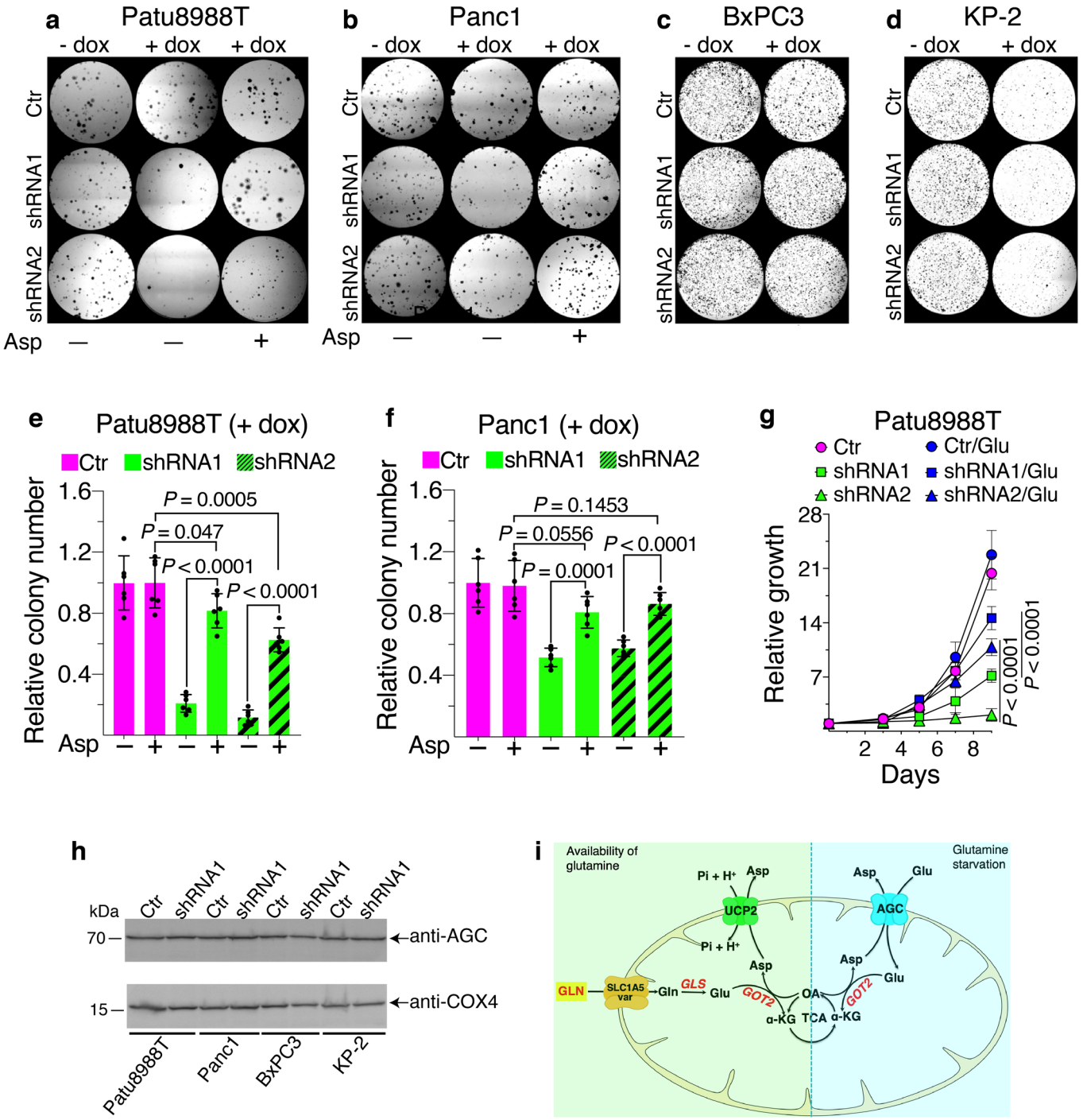

Extended Data Fig. 2 | UCP2 silencing reduces the availability of cytosolic aspartate in PDAC cell lines. a–f, UCP2 silencing reduces the clonogenic capacity of Patu8988T and Panc1 but not those of BxPC3 and KP-2 cells. The clonogenic assays corresponding to Fig. 1f are shown (**a**–**d**). Aspartate in the medium rescues the clonogenic defect of UCP2-silenced *KRAS*^{mut} PDAC cells (**a**, **b** and **e**, **f**). The histogram data were referred to dox-induced Ctr^{shRNA}-transfected cells without aspartate. **g**, The presence of glutamate (1 mM) in the medium partially rescues the proliferation defect induced by UCP2 silencing in *KRAS*^{mut} PDAC cells. Doxycycline was always present in **e**–**g**. **h**, UCP2 silencing does not alter the expression of the mitochondrial aspartate/glutamate carrier (AGC) in PDAC cells, similar results were obtained in three biologically independent experiments. COX4 normalization was carried out on the same SDS-PAGE used to assay AGC1/2 expression levels (**h**). **i**, An oversimplification of aspartate export out of mitochondria catalysed by UCP2 or AGC in the presence or limited availability of glutamine, respectively. Values represent means ± SD of two biologically independent triplicates. Statistical significance was calculated by unpaired two-tailed Student's *t*-test.

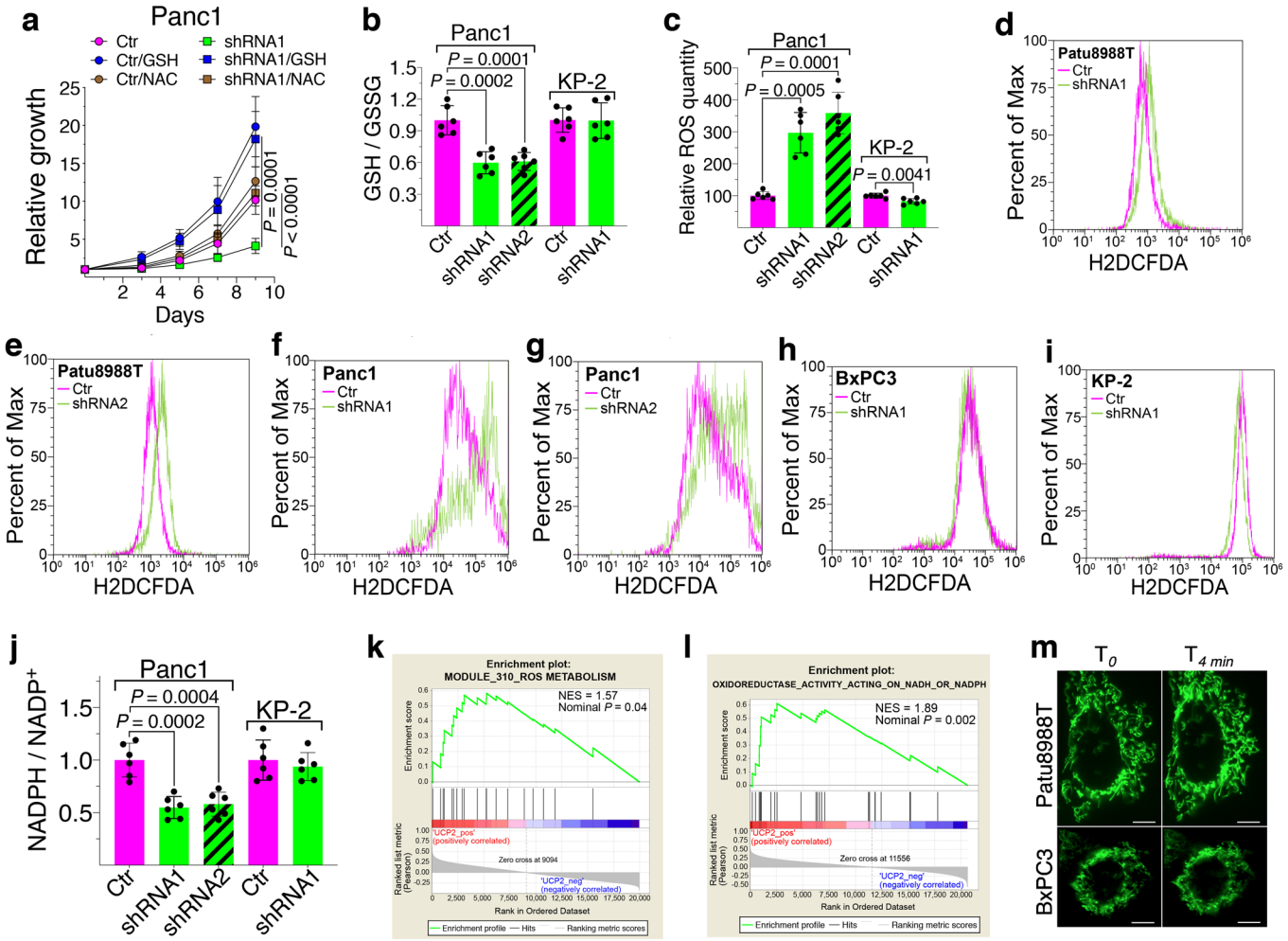

Extended Data Fig. 3 | UCP2 has key role in redox homeostasis of PDAC cells. a, GSH or NAC in the medium fully rescues the growth defect of UCP2-silenced Panc1 cells. **b**, UCP2 silencing reduces the GSH/GSSG ratio only in *KRAS*^{mut} cells. **c**–**i**, UCP2 silencing increases ROS levels only in *KRAS*^{mut} cells. The cytofluorimetric raw data of ROS analysis in control and UCP-silenced cells are shown (**d**–**i**). **j**, UCP2 silencing reduces the NADPH/NADP^{+} ratio only in *KRAS*^{MUT} cells. The histogram data were referred to Ctr^{shRNA}-transfected cells (**b**, **c** and **j**). **k, l**, In PDAC, *UCP2* expression levels are associated to those of genes involved in the redox homeostasis. The GSEA panels show the enrichment of gene sets related to *UCP2* expression in roughly 300 PDAC primary tumour samples from E-MTAB-6134 dataset (**k**) and 43 PDAC cell lines from dataset GSE36133 (**l**). NES, normalized enrichment score. **m**, Fluorescence microscopy images of mitochondrial-targeted GFP transfected Patu8988T and BxPC3 cells before and after 4 minutes of incubation with digitonin fractionation buffer. Scale bar = 10 μm. Values represent means ± SD of two biologically independent triplicates. Statistical significance was calculated by unpaired two-tailed Student's *t*-test; Welch correction was applied to shRNA1 *vs* shRNA1/GSH (**a**), Ctr *vs* shRNA1 and Ctr *vs* shRNA2 (Panc1) (**c**).

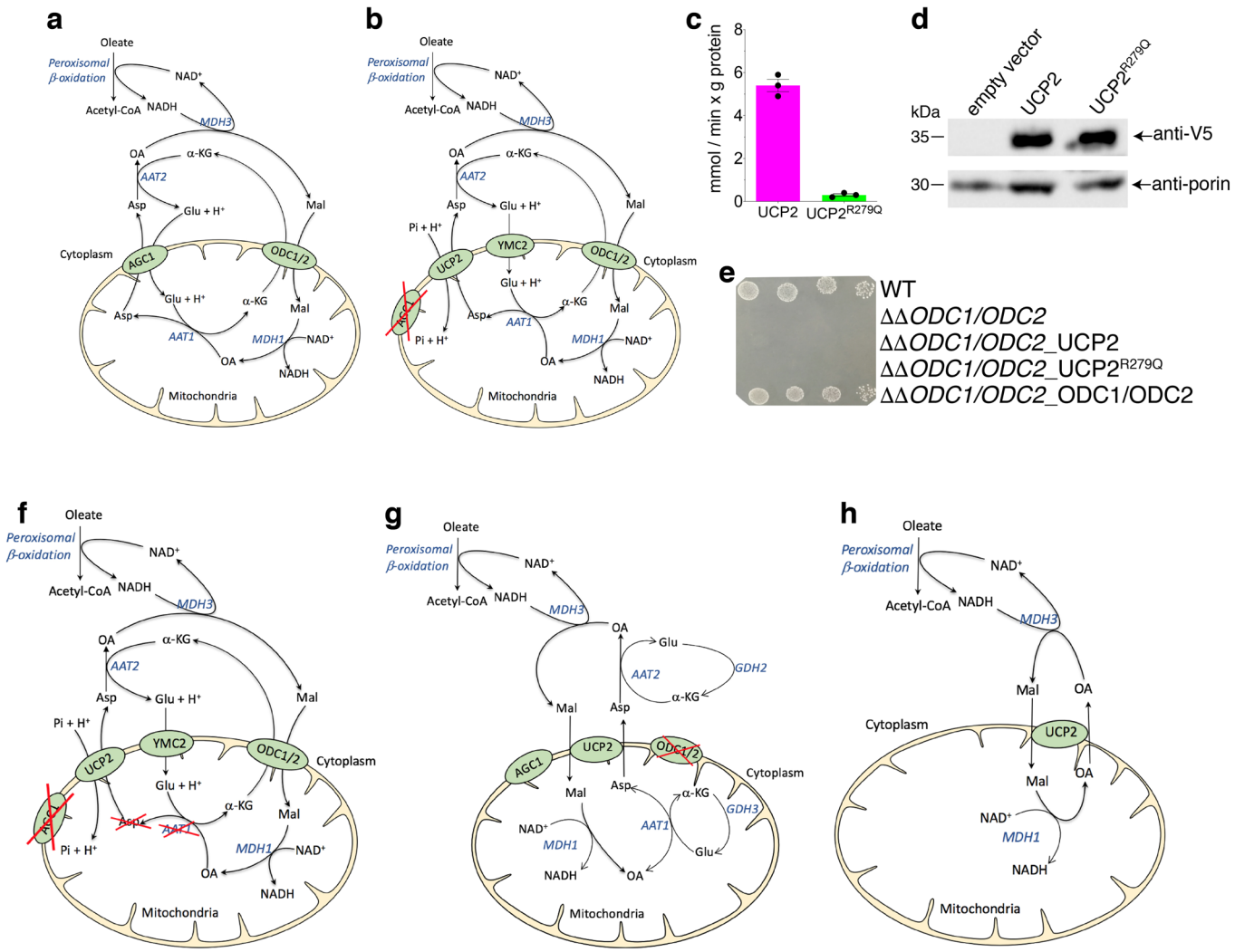

Extended Data Fig. 4 | In yeast cells, UCP2 catalyses the export of aspartate out of mitochondria in exchange for phosphate. a, The yeast mitochondrial aspartate/glutamate (AGC1p) and the two isoforms of oxoadipate carrier (ODC1p/ODC2p), which exchange 2-ketoglutarate against malate, are the mitochondrial carriers involved in the yeast malate-aspartate shuttle (MAS) required for the NADH oxidation derived from the peroxisomal oxidation of oleate. **b**, The UCP2 aspartate/Pi exchange activity together with the glutamate + H^+ symport catalysed by the yeast YMC2p restores the loss of AGC1p in MAS. **c**, The bacterial expressed $UCP2^{R279Q}$ mutant does not catalyse any aspartate/Pi exchange activity once reconstituted into liposomes. Values represent means ± SD of three independent experiments. **d**, A representative immunoblot of expression of UCP2 and $UCP2^{R279Q}$ V5-tagged proteins in W303 yeast cells used in panel **e**, similar results were obtained in three biologically independent experiments and in the yeast models reported in Fig. 2i–k. A yeast anti-porin antiserum was used for protein normalization. Porin normalization was carried out on the same SDS-PAGE used to assay V5-tagged UCP2 expression levels (**d**). **e**, Serial dilutions of different yeast cell models expressing UCP2 or $UCP2^{R279Q}$ were spotted on YP plate in the presence of oleate. **f**, To rescue the growth defect of the ΔAGC1 yeast strain on oleate, UCP2 requires the presence of the mitochondrial isoform of the aspartate transaminase (AAT1). **g, h**, In the inner mitochondrial membrane UCP2 catalyses only the aspartate/Pi exchange reaction. The two models show other two possible exchange activities catalysed by the recombinant UCP2 into liposomes, aspartate/malate and malate/oxaloacetate, which were not confirmed in the yeast models used. Asp, aspartate; Glu, glutamate; Mal, malate; α-KG, α-ketoglutarate; OA, oxaloacetate, MDH, malate dehydrogenase; GDH glutamate dehydrogenase.

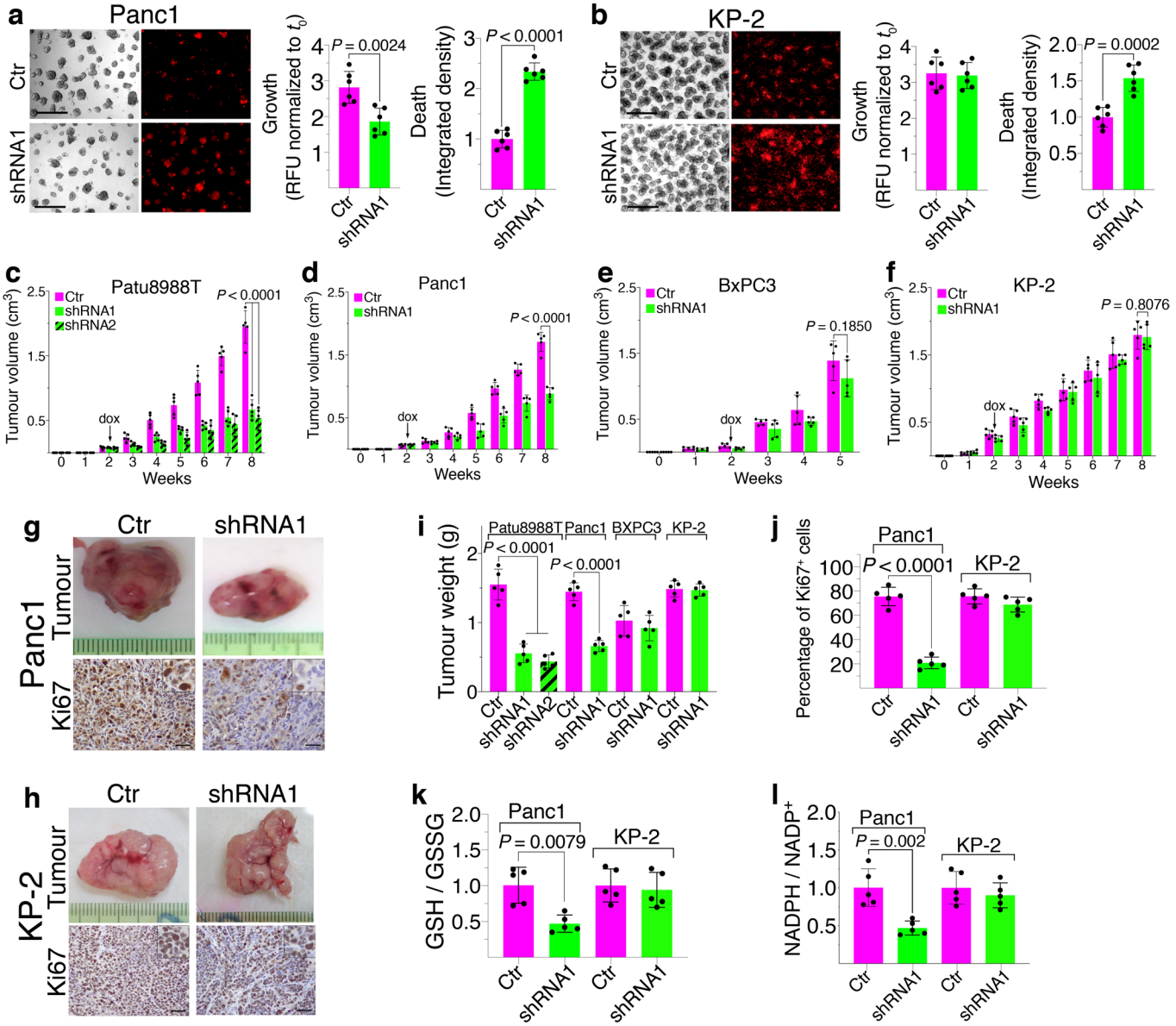

Extended Data Fig. 5 | UCP2 silencing inhibits *KRAS*^{mut} PDAC cells growth in organotypic 3D and xenograft models. a-b, UCP2 silencing reduces growth of organotypic cultures of *KRAS*^{mut} PDAC cells. Representative microscopic images of growth and death (red signal) of PDAC cells grown on 100% Matrigel ECM in the presence of doxycycline. Scale bar = 500 µm. Histograms show the growth and the death of cells cultured for seven days. The growth data were normalized to those measured at the beginning of the experiment (t_0), whereas the death data were referred to the Ctr^{shRNA}-transfected cells. **c-f**, UCP2 silencing inhibits the proliferation of *KRAS*^{mut} PDAC cells *in vivo*. The Patu8988T and BxPC3 tumour volumes reported in Fig. 3, panels **c** and **d** are shown (**c**, **e**). **g**, **h**, Representative images of tumour sizes and Ki67 immunostaining, taken at the end point, generated by Panc1 and KP-2 cells injected in female SCID mice (n = 5). Inset shows localization at higher magnification (40X), scale bar=25 µm (**g**, **h**). **i**, Tumour weights of all xenograft experiments. **j**, Percentage of Ki67 positive PDAC cells. **k, l**, UCP2 silencing reduces the GSH/GSSG and NADPH/NADP$^+$ ratios only in *KRAS*^{mut} cell xenografts, the histogram data were referred to Ctr^{shRNA} xenografts. Values represent means ± SD of two biologically independent triplicates (**a** and **b**) and five mice (**c**-**f** and **i**-**l**). Statistical significance was calculated by unpaired two-tailed Student's *t*-test (**a**-**f**, **i**, **j** and **l**) and unpaired two-tailed Mann–Whitney *U*-test (**k**). RFU, relative fluorescence unit.

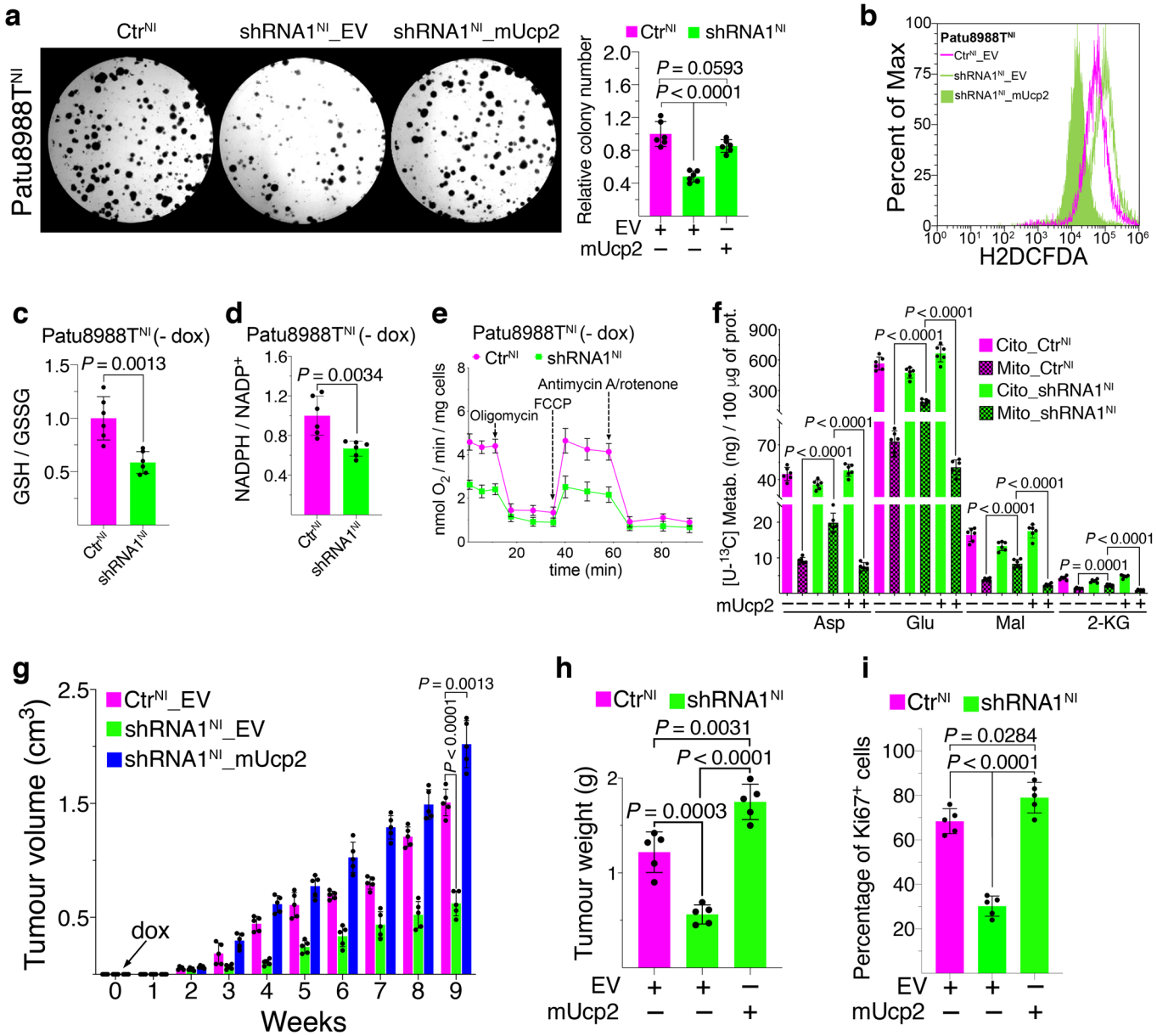

Extended Data Fig. 6 | Murine Ucp2 rescues the growth defect of UCP2-silenced *KRAS*^{mut} PDAC cells. a, mUcp2 expression rescues the clonogenic defect of UCP2-silenced *KRAS*^{mut} PDAC cells. **b**, Cytofluorimetric raw data of ROS analysis carried out in the rescue experiment reported in Fig. 4, panel **b**. **c, d**, UCP2 silencing reduces the GSH/GSSG and NADPH/NADP$^+$ ratios in Patu8988T^{NI} also in the absence of doxycycline, the histogram data were referred to the Ctr^{shRNA}-transfected cells. **e**, UCP2 silencing reduces oxygen consumption rates (OCR) in the presence of glutamine in Patu8988T^{NI} also in the absence of doxycycline, values represent means ± SD of three biologically independent experiments. **f**, mUcp2 expression recovers the altered cytosol/matrix distribution of the glutamine-derived metabolites of UCP2-silenced PDAC cells. **g-i**, Tumour volumes, tumour weights and the percentage of Ki67 positive cells of Patu8988T tumours reported in Fig. 4e are shown (n = 5). Asp, aspartate; Glu, glutamate; Mal, malate; 2-KG, 2-ketoglutarate. Patu8988T^{NI}, cells transfected with non-inducible lentiviral plasmids. Values represent means ± SD of two biologically independent triplicates (**a**, **c**, **d** and **f**) and five mice (**g-i**). Statistical significance was calculated by unpaired two-tailed Student's *t*-test. Welch correction was applied to Mito_Ctr^{NI} *vs* Mito_shRNA1^{NI} (Asp), Mito_Ctr^{NI} *vs* Mito_shRNA1^{NI} (Glu), Mito_shRNA1^{NI} *vs* Mito_shRNA1$^{NI(rescued)}$ (Glu) and Mito_shRNA1^{NI} *vs* Mito_shRNA1$^{NI(rescued)}$ (Mal) (**f**).

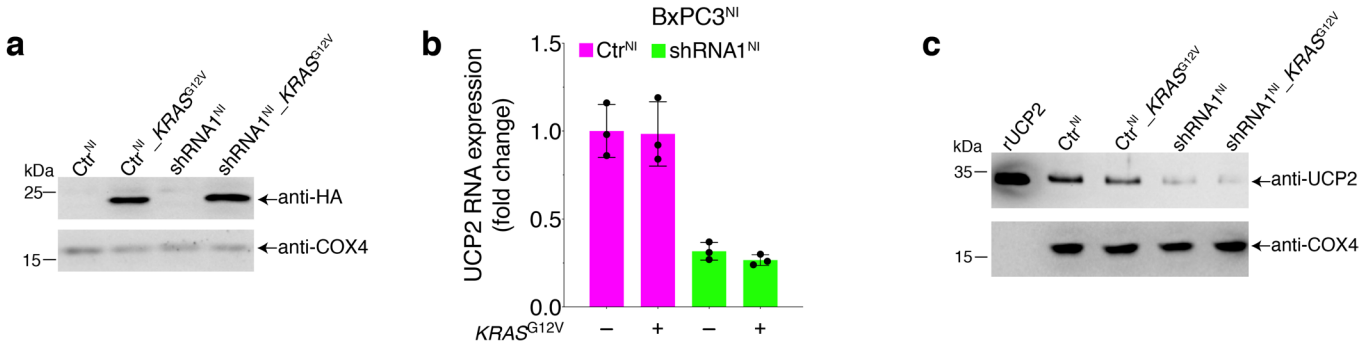

Extended Data Fig. 7 | Expression of *KRAS*^{G12V} in BxPC3 cells does not alter the expression levels of UCP2. a, Expression of HA-tagged *KRAS*$_{G12V}$ in control and UCP2^{shRNA}-transfected BxPC3 cells. **b, c** The relative expression of UCP2 in control and UCP2^{shRNA}-transfected BxPC3 cells expressing or not expressing *KRAS*^{G12V}. *UCP2* transcript levels were quantified by qPCR (**b**) and UCP2 protein levels were assayed with a UCP2-specific antiserum (**c**). An anti-COX4 antibody was used for norKP-2malization. COX4 normalization was carried out on the same SDS-PAGEs used to assay HA-tagged *KRAS*^{G12V} (**a**) and UCP2 (**c**) expression levels. Similar results were obtained in three biologically independent experiments (**a** and **c**). For transcript analyses, reverse transcribed cDNA from three biological replicates was used and three technical replicates were analysed for each biological replicate, values represent means ± SD of three independent experiments (**b**). BxPC3^{NI}, cells transfected with non-inducible lentiviral plasmids. rUCP2, recombinant human UCP2.

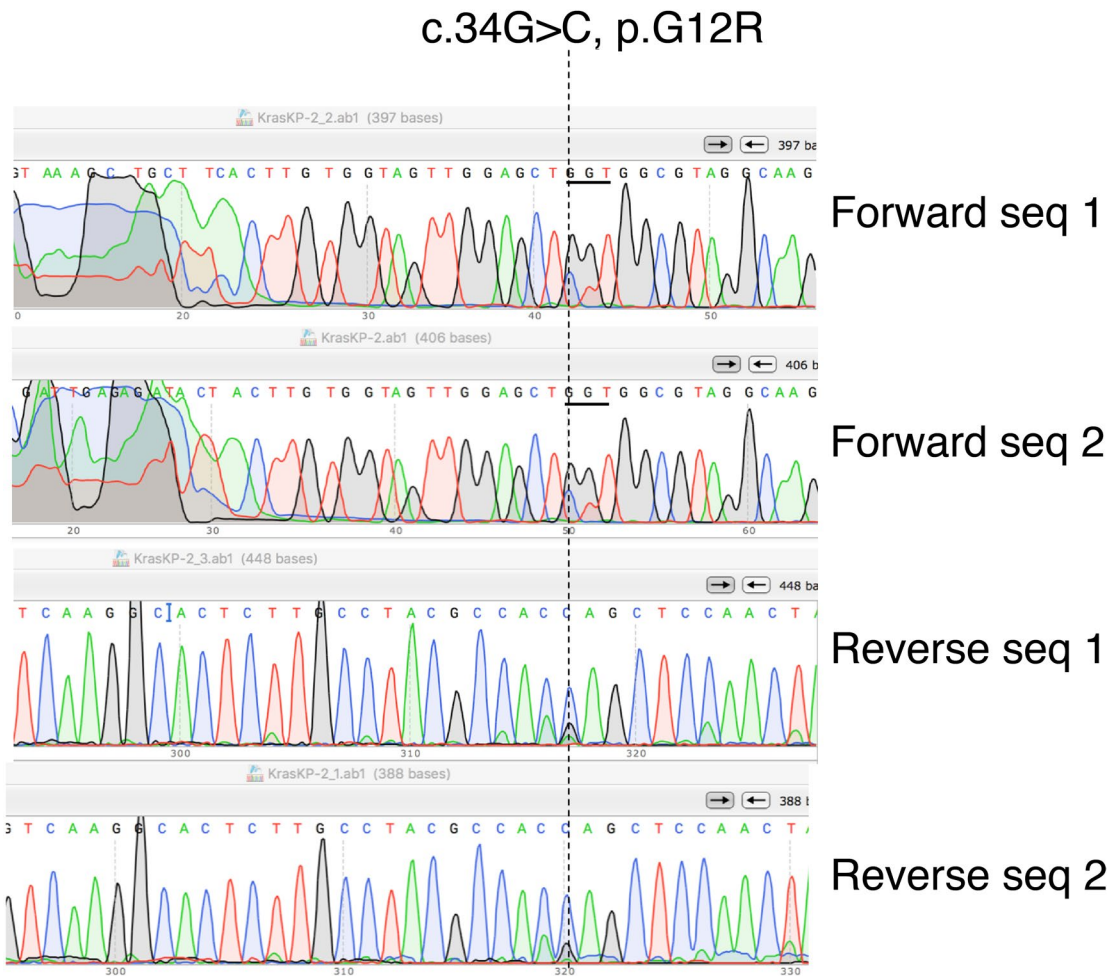

Extended Data Fig. 8 | KRAS allele imbalance in KP-2 PDAC cell lines. Two examples of forward and reverse sequences of PCR *KRAS* fragments (amplified from a first-strand cDNA) carried out along the study. The dotted line indicates difference in the pick's area between the wild-type sequence and the unverified heterozygous mutation (c.34G>C, p.G12R) found in the COSMIC database. The GGT codon encoding for the wild-type glycine 12 is underlined.

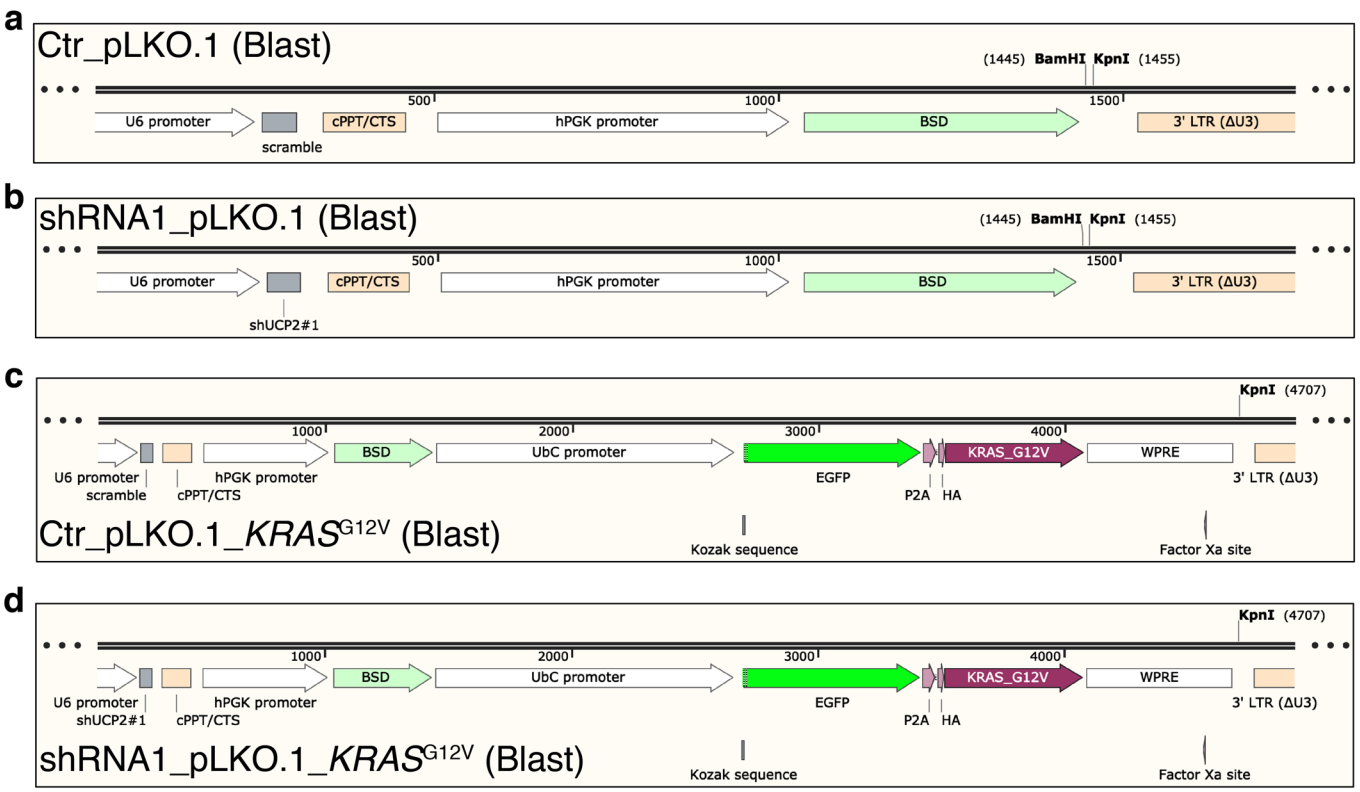

Extended Data Fig. 9 | A schematic representation of lentiviral plasmids used to verify the dependency of mutated *KRAS* on UCP2 in BxPC3 cells. a, **b**, The scramble and UCP2 silencing (shRNA1) non-inducible pLKO.1 (Blast) plasmids, used as controls, showing the BamHI and KpnI restriction sites used to clone the *KRAS*^{G12V} expression cassette. **c, d**, The scramble and UCP2 silencing (shRNA1) non-inducible pLKO.1 (Blast) plasmids carrying the *KRAS*^{G12V} expression cassette downstream the blasticidin resistance gene (BSD). HA-tagged *KRAS*^{G12V} was cloned under the control of the UbC promoter and in frame with EGFP and a "self-cleaving" P2A peptide. The efficiency of transfection (about 85%) was measured by following the EGFP fluorescence whereas the presence of P2A allowed the release of the HA-tagged *KRAS*^{G12V}.

nature research

Corresponding author(s): Giuseppe Fiermonte/Vincenza Dolce

Last updated by author(s): Sep 28, 2020

Reporting Summary

Nature Research wishes to improve the reproducibility of the work that we publish. This form provides structure for consistency and transparency in reporting. For further information on Nature Research policies, see Authors & Referees and the Editorial Policy Checklist.

Statistics

For all statistical analyses, confirm that the following items are present in the figure legend, table legend, main text, or Methods section.

n/a	Confirmed
☐	☒ The exact sample size (*n*) for each experimental group/condition, given as a discrete number and unit of measurement
☐	☒ A statement on whether measurements were taken from distinct samples or whether the same sample was measured repeatedly
☐	☒ The statistical test(s) used AND whether they are one- or two-sided *Only common tests should be described solely by name; describe more complex techniques in the Methods section.*
☐	☒ A description of all covariates tested
☐	☒ A description of any assumptions or corrections, such as tests of normality and adjustment for multiple comparisons
☐	☒ A full description of the statistical parameters including central tendency (e.g. means) or other basic estimates (e.g. regression coefficient) AND variation (e.g. standard deviation) or associated estimates of uncertainty (e.g. confidence intervals)
☐	☒ For null hypothesis testing, the test statistic (e.g. *F*, *t*, *r*) with confidence intervals, effect sizes, degrees of freedom and *P* value noted *Give P values as exact values whenever suitable.*
☒	☐ For Bayesian analysis, information on the choice of priors and Markov chain Monte Carlo settings
☒	☐ For hierarchical and complex designs, identification of the appropriate level for tests and full reporting of outcomes
☒	☐ Estimates of effect sizes (e.g. Cohen's *d*, Pearson's *r*), indicating how they were calculated

Our web collection on statistics for biologists contains articles on many of the points above.

Software and code

Policy information about availability of computer code

Data collection	A GS-800™ calibrated densitometer (BioRad) was used for Western blots acquisition. Seahorse XFe96 Analyzer (Agilent) and Wave Desktop 2.2 software were used for respirometry measurements. A Zeiss AxioVert 200 epifluorescence microscope and MetaMorph software 6.1 were used for mitochondrial integrity checking of permeabilised cells. A Waters® Micromass® Quattro micro™ GC Triple Quadrupole mass spectrometer, directly interfaced to an Agilent 6890N GC, was used for GC-MS analysis. Data were acquired and processed using MassLynx 4.0 software. Olympus BX51 microscope was used to acquire Ki67.
Data analysis	Data analysis and statistical tests were done using Prism (GraphPad Prism 7) or Excel 16.40 (Microsoft). Measurements for clonogenic assays and Ethidium Homodimer-1 assays were performed with ImageJ 1.8.0_172 (http://rsb.info.nih.gov/ij/). All GEP (HG-U133_Plus 2.0 and HG_U219 arrays from Affimetrix platform) were processed by using RMA (Robust Multi-array Average) with RMAExpress v1.2.0 software. The difference of UCP2 expression between PDAC samples and normal pancreas was determined by Mann-Whitney test with the R statistical programming environment (v3.4.3). qRT-PCR fluorescence data were calculated using the ABI SDS software 2.4 (Applied Biosystems). Mass spectra were analyzed by using MassLynx v4.0 software. Flow cytometry analysis was carried out using Attune™ NxT v2.6 Software.

For manuscripts utilizing custom algorithms or software that are central to the research but not yet described in published literature, software must be made available to editors/reviewers. We strongly encourage code deposition in a community repository (e.g. GitHub). See the Nature Research guidelines for submitting code & software for further information.

Data

Policy information about availability of data

All manuscripts must include a data availability statement. This statement should provide the following information, where applicable:

- Accession codes, unique identifiers, or web links for publicly available datasets
- A list of figures that have associated raw data
- A description of any restrictions on data availability

All data used for expression analysis and GSEA were publicly available.

The datasets using HG133plus2 from Affymetrix included
1. E-MEXP-2780 (https://www.ebi.ac.uk/arrayexpress/experiments/E-MEXP-2780/);
2. GSE15471 (https://www.ncbi.nlm.nih.gov/geo/download/?acc=GSE15471&format=file);
3. GSE22780 (https://www.ncbi.nlm.nih.gov/geo/download/?acc=GSE22780&format=file);
4. GSE16515 (https://www.ncbi.nlm.nih.gov/geo/download/?acc=GSE16515&format=file);
5. GSE32676 (https://www.ncbi.nlm.nih.gov/geo/download/?acc=GSE32676&format=file);
6. GSE42952 (https://www.ncbi.nlm.nih.gov/geo/download/?acc=GSE42952&format=file);
7. GSE36133 (https://www.ncbi.nlm.nih.gov/geo/download/?acc=GSE36133&format=file);
The dataset using HG_U219 from Affymetrix included E-MTAB-6134 (https://www.ebi.ac.uk/arrayexpress/experiments/E-MTAB-6134/)
The row data of Figures 2 and 4 (ROS analysis) have been reported in Extend Data Fig. 3, panels, d-i and Extend Data Fig. 6, panel b, respectively. The gating strategies used for ROS analysis has been reported in Supplementary Figure 1. The COSMIC database link where it is reported an unverified heterozygous mutation (c.34G>C, p.G12R) for KP2 cells is https://cancer.sanger.ac.uk/cell_lines/sample/overview?id=1298218. There no restriction on data availability, any additional information supporting the data within this paper and the findings of this study are available from the corresponding authors upon request.

Field-specific reporting

Please select the one below that is the best fit for your research. If you are not sure, read the appropriate sections before making your selection.

☒ Life sciences ☐ Behavioural & social sciences ☐ Ecological, evolutionary & environmental sciences

For a reference copy of the document with all sections, see nature.com/documents/nr-reporting-summary-flat.pdf

Life sciences study design

All studies must disclose on these points even when the disclosure is negative.

Sample size	No sample-size calculations were performed. Sample size was determined to be adequate based on the magnitude and consistency of measurable differences between groups. On the basis of previous studies using related experiments, the sample size has been determined to be sufficient to ensure reproducibility by performing three technical replicates of two biologically independent experiments.
Data exclusions	Data were only excluded for failed experiments, i.e. if the researcher realized that a technical error occurred accidentally during the execution of experiment.
Replication	All experiments were repeated at least twice to ensure reproducibility. Replication numbers (3 for each experiment) are reported in the figures as scatter plots with bar or in the Methods section as required.
Randomization	No randomization of mice. All Mice analyzed were sex-matched. For all other experiments and measurements, sample identity was not randomized.
Blinding	For mice studies, tumour development and staining intensity of tissue sections were scored in a 'blinded' manner. Blinding was also used only for GC-MS studies since the execution and data analysis of the other experiments were usually carried out by the same investigator.

Reporting for specific materials, systems and methods

We require information from authors about some types of materials, experimental systems and methods used in many studies. Here, indicate whether each material, system or method listed is relevant to your study. If you are not sure if a list item applies to your research, read the appropriate section before selecting a response.

Materials & experimental systems

n/a	Involved in the study
☐	☒ Antibodies
☐	☒ Eukaryotic cell lines
☒	☐ Palaeontology
☐	☒ Animals and other organisms
☒	☐ Human research participants
☒	☐ Clinical data

Methods

n/a	Involved in the study
☒	☐ ChIP-seq
☐	☒ Flow cytometry
☒	☐ MRI-based neuroimaging

Antibodies

Antibodies used	V5-Tag (D3H8Q) Rabbit mAb #13202 (Cell Signaling), yeast porin (VDAC1) antiserum (De Marcos Lousa, C., Trezeguet, V., Dianoux, A. C., Brandolin, G. & Lauquin, G. J. The human mitochondrial ADP/ATP carriers: kinetic properties and biogenesis of wild-type and mutant proteins), COX4 Antibody (F-8) (sc-376731, Santa Cruz Biotechnology), purified anti-HA.11 epitope, clone 16B12 (Cat.n. 901501, BioLegend), Goat anti-Rabbit IgG (H+L) Secondary Antibody, HRP (ThermoFisher Scientific Pierce™ # 31460), Goat anti-Mouse IgG (H+L) Secondary Antibody, HRP (ThermoFisher Scientific Pierce™ # 31430) and homemade murine

UCP2 and rabbit AGC antibodies were used in the study.

Validation

The anti-V5-Tag antibody (Cell Signaling #13202) has been validated by the manufacturer by Western blot analysis carried out on human COS-7 cell lysate, untransfected (-) or transfected with V5-tag fusion protein and it has been cited in 82 papers (https://www.cellsignal.com/products/primary-antibodies/v5-tag-d3h8q-rabbit-mab/13202?Ntk=Products&Ntt=13202). The anti-COX4 antibody (F-8) (sc-376731, Santa Cruz Biotechnology) has been validated by the manufacturer by Western blot analysis carried out on A-431, MOLT-4, Raji, MCF7 and A-673 whole cell lysates and human skeletal muscle tissue extracts and it has been cited in 39 papers (https://www.scbt.com/p/cox4-antibody-f-8). The anti-Anti-HA.11 epitope, clone 16B12 (Cat.n. 901501, BioLegend) recognizes the influenza hemagglutinin epitope (YPYDVPDYA) which has been used extensively as a general epitope tag in expression vectors. The extreme specificity of the antibody allows unambiguous identification and quantitative analysis of the tagged protein. Its validation has been also confirmed in the results reported in Extended Data Fig. 7a in which the antibody reacted only against samples expressing the HA-KRAS. The antibody against the yeast Porin (VDAC1, POR1, YNL055C) was successfully used by C. De Marcos Lousa, et al. (Biochemistry 41 (2002) 14412-14420). The antibody has been also validated in our laboratory, since it reacts against the bacterial recombinant protein and gives no reaction against mitochondrial extracts derived from a yeast strain in which the POR1 gene had been deleted. The home-made murine UCP2 antibody has been validated in our laboratory against the murine and human recombinant UCP2 as also shown in Extended Data Fig. 1c and 1i and 7c. The homemade rabbit antibody against AGC1/2 was validated against the human and murine bacterial recombinant mitochondrial aspartate/glutamate carrier isoforms 1 and 2 (AGC1 and AGC2).

Eukaryotic cell lines

Policy information about cell lines

Cell line source(s)

Patu8988T (ACC 162), Panc1 (CRL-1469) and BxPC3 (CRL-1687) were from ATCC and KP2 (JCRB0181) from JCRB Cell Bank

Authentication

All STR profiles of human PDAC cell lines have been verified at Boehringer Ingelheim RCV GmbH & Co KG, Vienna, Austria. The allelic imbalance in favour of wild-type allele (GGT, glycine at position 12 vs CGT, arginine, in KRAS ORF) in the KP2 cell line has been verified by PCR fragment sequencing (amplified from a first-strand cDNA) carried out along the study (Extended Data Fig. 8).

Mycoplasma contamination

All cell lines used were regularly tested for mycoplasma and were found to be mycoplasma free.

Commonly misidentified lines
(See ICLAC register)

No commonly misidentified cell lines were used in this study

Animals and other organisms

Policy information about studies involving animals; ARRIVE guidelines recommended for reporting animal research

Laboratory animals

5 weeks old female SCID mice C.B-17/IcrHanHsd-Prkdcscid congenic strain of Balb/cAnIcr were used in this study and were purchased from ENVIGO RMS srl, (Udine, Italy). The mice were housed with 12-hour light/dark cycle at 23±1°C and 50±5 % humidity, and ad libitum diet and water were provided. The endpoint of experiments was usually 7-9 weeks later cell injection when the tumour volume was about 1.5-2 cm3.

Wild animals

No wild animals were used in this study

Field-collected samples

No field-collected samples were used in this study.

Ethics oversight

Xenograft experiments with human PDAC lines were approved by Italian Ministry of Health under protocol number 418/2015-PR. All animals were maintained and handled in accordance with the recommendation of the Guidelines for the Care and Use of Laboratory Animals and experiments were approved by the Animal Care Committee of University of Calabria (OPBA), Italy

Note that full information on the approval of the study protocol must also be provided in the manuscript.

Flow Cytometry

Plots

Confirm that:

☒ The axis labels state the marker and fluorochrome used (e.g. CD4-FITC).

☒ The axis scales are clearly visible. Include numbers along axes only for bottom left plot of group (a 'group' is an analysis of identical markers).

☒ All plots are contour plots with outliers or pseudocolor plots.

☒ A numerical value for number of cells or percentage (with statistics) is provided.

Methodology

Sample preparation

The four human PDAC cell lines were plated in their specific media with doxycycline. The next day, medium were changed with D-5030 medium supplemented with 2 mM glutamine, 10 mM glucose, 10% dFBS and doxycycline. After four days 2 x 10^5 cells per sample were stained with 10 µM 2',7'-dichlorodihydrofluorescein diacetate (H2DCFDA, Molecular Probes, Eugene) for 30

	min at 37°C. After staining, the cells were washed and measured.
Instrument	Attune Nxt Acoustic Focusing Cytometer (Life Technologies Corporation).
Software	Analysis was performed and data visualized using the Attune™ NxT v2.6 Software.
Cell population abundance	Cellular sorting was not been conducted
Gating strategy	Full gating strategy was been conducted.

☒ Tick this box to confirm that a figure exemplifying the gating strategy is provided in the Supplementary Information.